Available online at www.sciencedirect.com

ScienceDirect

Advances in Space Research 54 (2014) 1838–1857

ADVANCES IN SPACE RESEARCH (a COSPAR publication)

www.elsevier.com/locate/asr

Zero, minimum and maximum relative radial acceleration for planar formation flight dynamics near triangular libration points in the Earth–Moon system ☆

F.J.T. Salazar [a,*], J.J. Masdemont [b], G. Gómez [c], E.E. Macau [d], O.C. Winter [a]

[a] UNESP-Grupo de Dinâmica Orbital e Planetologia, Guaratinguetá, SP 12516-410, Brazil
[b] Departament de Matemàtica Aplicada I, ETSEIB-UPC, Avda. Diagonal 647, 08028 Barcelona, Spain
[c] Departament de Matemàtica Aplicada i Anàlisi, UB, Gran Vía 585, 08007 Barcelona, Spain
[d] Instituto Nacional de Pesquisas Espaciais, Av. dos Astronautas 1758, São José dos Campos, SP 12227-010, Brazil

Received 6 April 2014; received in revised form 17 July 2014; accepted 20 July 2014
Available online 26 July 2014

Abstract

Assume a constellation of satellites is flying near a given nominal trajectory around L_4 or L_5 in the Earth–Moon system in such a way that there is some freedom in the selection of the geometry of the constellation. We are interested in avoiding large variations of the mutual distances between spacecraft. In this case, the existence of regions of zero and minimum relative radial acceleration with respect to the nominal trajectory will prevent from the expansion or contraction of the constellation. In the other case, the existence of regions of maximum relative radial acceleration with respect to the nominal trajectory will produce a larger expansion and contraction of the constellation. The goal of this paper is to study these regions in the scenario of the Circular Restricted Three Body Problem by means of a linearization of the equations of motion relative to the periodic orbits around L_4 or L_5. This study corresponds to a preliminar planar formation flight dynamics about triangular libration points in the Earth–Moon system. Additionally, the cost estimate to maintain the constellation in the regions of zero and minimum relative radial acceleration or keeping a rigid configuration is computed with the use of the residual acceleration concept. At the end, the results are compared with the dynamical behavior of the deviation of the constellation from a periodic orbit.

Keywords: Formation flight of satellites; Zero Relative Radial Acceleration; Earth–Moon system; Circular Restricted Three Body Problem; Stable Lagrangian points; Residual acceleration

1. Introduction

The concept of Satellite Formation Flying (SFF) means to have two or more satellites in orbit such that their relative positions remain constant or obeying a certain dynamical configuration along the trajectory (Sholomitsky et al., 1977; Battrick, 2000; Bristow et al., 2000; Burns et al., 2000; Ticker and Azzolini, 2000; Fridlund and Capaccioni, 2002). This concept involves the control over the coordinated motion of a group of satellites, with the goal of maintaining a specific geometric space configuration between the elements of the cluster (Sabol et al., 2001). It allows that a group of low cost small satellites, arranged in a space formation flying, operate like a large 'virtual satellite'. This formation will have many benefits over single satellites, including simpler designs, faster build

☆ This template can be used for all publications in Advances in Space Research.

* Corresponding author. Tel.: +55 12 981015572.
E-mail addresses: e7940@hotmail.com (F.J.T. Salazar), josep@barquins.upc.edu (J.J. Masdemont), gerard@maia.ub.es (G. Gómez), elbert.macau@inpe.br (E.E. Macau), ocwinter@gmail.com (O.C. Winter).

http://dx.doi.org/10.1016/j.asr.2014.07.018
0273-1177/

times, cheaper and unprecedented high resolution (Kapila et al., 2000). Over the past decade, numerous formation flying missions have been conceived. The Laser Interferometer Space Antenna (LISA) is a proposed mission, whose objective is to observe astrophysical and cosmological sources of gravitational waves of low frequencies, goal that could be possible using three identical spacecraft flying in a triangular constellation, with equal arms of 5 million kilometers each (Peterseim et al., 2000). Another example is the PRISMA formation flying and rendezvous technology mission, launched successfully on June 25, 2010, into a Sun synchronous orbit at approximately 750 km altitude (Persson et al., 2006; Gill et al., 2007; Hellman et al., 2009; Persson et al., 2010). PRISMA mission consists of two spacecraft: Mango and Tango, with a total mass of about 200 kg, and its primary purpose is to demonstrate formation flying and rendezvous technology, not only in terms of Guidance, Navigation and Control software and algorithms, but also in terms of instruments and operational aspects (e.g., small rocket engines and Micro Electro Mechanical Systems). Another interesting formation flying mission is the New Worlds Observer (NWO) (Cash et al., 2009). NWO consists of a large telescope and an occulter spacecraft in tandem at about 50,000 km apart. The two spacecraft would be flying at the Earth–Sun L_2 Lagrangian point or in a drift-away solar orbit. Its purpose is to discover and analyze terrestrial extra-solar planets. The NWO planned launch date is about 2018.

A configuration of SFF can typically be positioned and maintained in two dynamically distinct scenarios: in a planetary orbit or in outer space (Alfriend et al., 2002). In the planetary orbit scenario the fundamental model is the problem involving two light bodies (satellites), close to each other, that could be in the same orbit or describe orbits of slightly different radii, eccentricities and inclinations around a massive central body, e.g. the Earth. Because the gravitational attraction between the two satellites is negligible, this scenario can be considered like a superposition of two problems of two bodies (Sengupta and Vadali, 2007), where the atmospheric drag and higher-order gravity terms (e.g., J_2) can be considered in the dynamic models of the formation (Carter and Humi, 2002; Humi and Carter, 2006; Sengupta et al., 2007) and, therefore, improving the fidelity of the model. An example of this kind of formation is the pair of satellites Landsat 7 with EO-1, mission designed to enable the development of future Earth imaging observatories that will have a significant increase in performance while reducing cost and mass (Flick, 2012).

In the outer space scenario, involving SFF in the vicinity of a libration point, the fundamental model to study the natural motion of spacecraft relative to each other is the Circular Restricted Three Body Problem (CRTBP) (Hsiao and Scheeres, 2002). The interest of astronomical missions has been to position SFF around the Lagrangian points L_1 and L_2 (Faquhar, 1968; Henon, 1973; Breakwell and Brown, 1979; Howell, 1984; Gómez et al., 2000) or L_4 and L_5. Of particular interest is the stability of the five Lagrangian points. In the case of the three collinear stationary points: L_1, L_2 and L_3, they are always unstable. Whereas the stability of L_4 and L_5 points depends on the mass ratio between the two larger bodies (Danby, 1962; Szebehely, 1967). In important cases like Earth–Moon or Sun–Earth, these points are linearly stable. Moreover, there exists a family of periodic orbits around L_4 and L_5. This stability property makes the fuel required for a spacecraft to maintain its relative position there to be almost zero. Despite this advantage, today there are no missions orbiting L_4 or L_5 points for any celestial pair of primaries. In the case of Earth–Moon system, L_4 and L_5 points could be excellent locations to place space telescopes for astronomical observations or a space station (Schutz et al., 1977). In addition, there is a renewed interest of major space agencies for Lagrangian point colonization. Furthermore, Defilippi (1977) has made a review of the ideas of O'Neill (1974) about building space colonies at the L_4 and L_5 positions. These space stations could be used as a way-point for traveling to and from the region between Earth's atmosphere and the Moon (cis-lunar space).

For the reason that keeping a formation from drifting apart and achieving mission requirements is expected to require significantly more fuel than station keeping a single spacecraft, one of the problems of positioning satellites in formation flying is the cost to maintain them continuously orbiting each other. In particular, missions in the vicinity of the Lagrangian points, considering the scenario of the CRTBP, may be placed in families of halo orbits. All these orbits are inherently unstable (Gómez et al., 1993) and drive the SFF out of its desired configuration. Thereby, a less difficult option is to place the Satellite Formation Flying in the vicinity of Earth–Moon L_4 and L_5 Lagrangian points. Because of their stability properties, less fuel would be spent to keep the formation in its proper configuration.

Previous studies like those by Catlin and McLaughlin (2007) and Wong (2009) on SFF about L_4 in the Earth–Moon system have been analyzed. The motion of formation flying near triangular libration points was studied adopting the CRTBP model and the linearized equations at the equilibrium points. Catlin and McLaughlin (2007) show that formations are possible at the Triangular points on uncontrolled trajectories due to the stability of stationary solutions. On the other hand, Wong (2009) establishes the need for a system control and develops strategies for controlling a spacecraft formation system at the L_4. In the CRTBP scenario, these studies show that velocity change requirements demanded by the control methods would be very small. Thus, Catlin and McLaughlin (2007) and Wong (2009) conclude that nonlinear aspects as well as perturbations forces (e.g. solar gravity, solar radiation pressure) are necessary to provide a more real-world accurate descriptions of motion and control of formation flying around equilateral equilibrium points in the Earth–Moon system.

In this work, we do not adopt the linear model about L_4, we investigate the relative dynamical behavior of satellites with respect to periodic orbits around L_4 and L_5 in the

Earth–Moon system and look for stable regions with good properties for formation flying. In particular, we are interested in finding relative positions of the formation with respect to the periodic orbits such that large variations of the mutual distance between satellites are avoided. In this manner, supposing that the relative velocity of each satellite with respect to the periodic orbit is zero, the regions with good properties for formation flying are such that the relative radial acceleration with respect to the periodic orbit is zero (Gómez et al., 2006). We present analytical and numerical methods based on the linearization of the relative equations of motion with respect to periodic orbits to find the regions where the radial component of the relative acceleration is zero. Gómez et al. (2006) applied a similar methodology for halo orbits around the collinear equilibrium point L_2 in the Sun–Earth system, which are unstable, and showing the existence of regions of Zero Relative Radial Acceleration for halo orbits. In our case, we are interested in investigating the existence of these regions for a planar formation flight dynamics near periodic orbits around the equilateral equilibrium points L_4 and L_5 in the Earth–Moon system. Additionally, the cost to maintain a formation in these regions or keeping a rigid configuration is analyzed according to the residual acceleration concept as well as the expansion or contraction of the configuration. In this study, we consider the scenario of CRTBP assuming that all spacecraft's trajectories lie on the same orbital plane, such that, Moon's eccentricity and perturbations from Sun will be neglected. This simplified model offers a good first approximation for the planar formation flight dynamics about triangular libration points. However, since perturbations from Moon and Sun affect the stability of triangular libration points (Schechter, 1968; Kamel and Breakwell, 1970; Tapley and Schultz, 1970; Gómez et al., 1987; Gómez et al., 2001; McLaughlin et al., 2004), they will be considered in subsequent works, obtaining a more accurate model, which is important for practical purposes.

This article proceeds as follows: In Section 2, we describe the equations of motion of the formation on the plane close to periodic orbits around L_4 and L_5; next, in Section 3, we describe the analytical and numerical methods to determine the regions of Zero Relative Radial Acceleration as well as we define mathematically the residual acceleration concept. In Section 4, we determine the regions of Zero, minimum and maximum relative radial acceleration for two kinds of periodic orbit families. In Sections 5 and 6, we estimate the cost to maintain a spacecraft on these regions and keeping a rigid configuration, respectively. In Section 7, we study the dynamical behavior of the distance between the spacecraft and the periodic orbits for different initial conditions; and finally, in Section 8, we present our conclusions on the study.

2. Equations of local dynamics of satellite formation flying

In this section we describe a linear approach to the problem of formation flying that gives the relevant information about the local dynamics of the problem. In order to avoid expansion or contraction in a constellation of spacecraft, we have studied the existence of regions with Zero Relative Radial Acceleration (ZRRA). For a simple model, such as the CRTBP, it is possible to compute an analytical expression for these regions. If the radius of the constellation (largest separation between spacecraft) is small, then a linear approach gives all the relevant information about the local dynamics of the problem (Gómez et al., 2006). As a first approximation to study the natural motion of spacecraft relative to each other near periodic orbits around L_4, our model only considers motions on the plane of the orbit of the Earth–Moon system. As reference solutions, we will use families of periodic orbits around L_4 since the results obtained are the same for periodic orbits around L_5 due to the Mirror Image Theorem applied in the Earth–Moon system (Miele, 1960). Considering the sum of the masses of the two primaries, the distance between them and also making the Newton's gravitational constant equal the one, in a frame rotating with the primaries, the equations of motion for a spacecraft in the non-dimensional variables are:

$$\ddot{x} - 2\dot{y} = \frac{\partial U}{\partial x}, \tag{1}$$

$$\ddot{y} + 2\dot{x} = \frac{\partial U}{\partial y}, \tag{2}$$

where $U = U(x, y)$ is given by

$$U(x,y) = \frac{1}{2}\left(x^2 + y^2\right) + \frac{1-\mu}{\rho_1} + \frac{\mu}{\rho_2} + \frac{1}{2}\mu(1-\mu) \tag{3}$$

and the non-dimensional relative distance ρ_i is defined as

$$\rho_i = \sqrt{(x - x_i)^2 + y^2}. \tag{4}$$

Let $X = (x, y, \dot{x}, \dot{y})^T$ be the vector that describes the position and velocity of the mass m. Hence the equations of motion (1) and (2) can be written in vector form as

$$\dot{X} = \boldsymbol{f}(X), \tag{5}$$

where

$$\boldsymbol{f} = \begin{pmatrix} \dot{x} \\ \dot{y} \\ 2\dot{y} + \frac{\partial U}{\partial x} \\ -2\dot{x} + \frac{\partial U}{\partial y} \end{pmatrix}. \tag{6}$$

Now assume a formation such that the chief satellite is placed in a periodic orbit around L_4 as show in Fig. 1. Let $X_h(t)$ and $X(t)$ be the vectors corresponding to the trajectories of the chief and deputy satellites, respectively. Then the vector $\Delta X(t) = X(t) - X_h(t)$ represents the relative position and velocity vectors of the deputy satellite with respect to the chief satellite at instant t. The coordinates of vector $\Delta X(t)$ are defined in a coordinate system x', y' parallel to the rotating coordinate system x, y and centered at $X_h(t)$ (see Fig. 1).

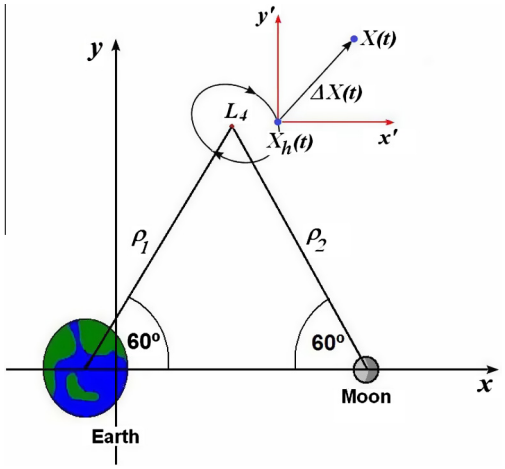

Fig. 1. Illustration of a satellite formation flying about L_4. $X_h(t)$ and $X(t)$ denote the corresponding trajectories of the chief and deputy satellites, respectively. $\Delta X(t)$ represents the relative position and velocity of the deputy satellite at instant t with respect to a coordinate system $\hat{x}$, $\hat{y}$ parallel to the rotating coordinate system x, y and centered at $X_h(t)$.

Differentiating the vector ΔX with respect to time t, we have

$$\Delta\dot{X} = \dot{X} - \dot{X}_h = \boldsymbol{f}(X) - \boldsymbol{f}(X_h). \tag{7}$$

Supposing that the diameter of the formation (largest separation between the spacecraft) is small compared with the chief's distances with respect to the Earth and the Moon, ρ_1 and ρ_2, respectively, then we can linearize the vector field $\boldsymbol{f}(X)$ around the periodic orbit $X_h(t)$ (Hill, 1878; Clohessy and Wiltshire, 1960)

$$\boldsymbol{f}(X) \approx \boldsymbol{f}(X_h) + D\boldsymbol{f}(X_h)\Delta X. \tag{8}$$

Substituting this expression in Eq. (7), we obtain the linear behavior of the deputy satellite around a periodic solution:

$$\Delta\dot{X} = D\boldsymbol{f}(X_h)\Delta X, \tag{9}$$

where

$$D\boldsymbol{f} = \begin{pmatrix} 0 & 0 & 1 & 0 \\ 0 & 0 & 0 & 1 \\ \frac{\partial^2 U}{\partial x^2} & \frac{\partial^2 U}{\partial y \partial x} & 0 & 2 \\ \frac{\partial^2 U}{\partial x \partial y} & \frac{\partial^2 U}{\partial y^2} & -2 & 0 \end{pmatrix}. \tag{10}$$

3. Zero Relative Radial Accelerations Lines

Assume two satellites flying in a formation in a periodic orbit around L_4. Writing the array ΔX as $(\boldsymbol{r}, \dot{\boldsymbol{r}})^T$, where $\boldsymbol{r} = (\Delta x, \Delta y)^T$, the linear system (9) becomes

$$\begin{pmatrix} \dot{\boldsymbol{r}} \\ \ddot{\boldsymbol{r}} \end{pmatrix} = \begin{pmatrix} 0 & I \\ F & J \end{pmatrix} \begin{pmatrix} \boldsymbol{r} \\ \dot{\boldsymbol{r}} \end{pmatrix}, \tag{11}$$

where

$$I = \begin{pmatrix} 1 & 0 \\ 0 & 1 \end{pmatrix}, \quad J = \begin{pmatrix} 0 & 2 \\ -2 & 0 \end{pmatrix}, \quad F = \begin{pmatrix} \frac{\partial^2 U}{\partial x^2} & \frac{\partial^2 U}{\partial y \partial x} \\ \frac{\partial^2 U}{\partial x \partial y} & \frac{\partial^2 U}{\partial y^2} \end{pmatrix}.$$

The points with zero relative velocity are those such that $\dot{\boldsymbol{r}} = \boldsymbol{0}$, and, in this case, we have that the relative acceleration is given by

$$\ddot{\boldsymbol{r}} = F\boldsymbol{r}. \tag{12}$$

Therefore, the radial component of the relative acceleration will be zero in the set of points where the vectors $\ddot{\boldsymbol{r}}$ and $\dot{\boldsymbol{r}}$ are orthogonal, in other words,

$$\boldsymbol{r}^T F \boldsymbol{r} = 0. \tag{13}$$

Eq. (13) represents two lines which depend on the point $X_h(t)$ selected along the periodic solution of system (5).

Zero Relative Radial Acceleration Lines (ZRRAL) can also be computed numerically (Gómez et al., 2006). Given a certain periodic orbit, we select a point on it: $X_h(t) = (\boldsymbol{x_h}(t), \boldsymbol{v_h}(t))^T$. Around this point, we consider a sphere in the configuration space, of radius s and we set the velocity of all the points of the sphere equal to the velocity of the chosen point, $\boldsymbol{v_h}(t)$ (zero relative velocity condition). Using polar coordinates, the set of points on the sphere are given by

$$\begin{pmatrix} \boldsymbol{x_h}(t) + \boldsymbol{s}(\theta) \\ \boldsymbol{v_h}(t) \end{pmatrix}. \tag{14}$$

Now, writing the equations of the motion (5) for X_h as

$$\begin{pmatrix} \dot{\boldsymbol{x}}_h \\ \ddot{\boldsymbol{x}}_h \end{pmatrix} = \begin{pmatrix} \boldsymbol{f_1}(\boldsymbol{x_h}, \boldsymbol{v_h}) \\ \boldsymbol{f_2}(\boldsymbol{x_h}, \boldsymbol{v_h}) \end{pmatrix}, \tag{15}$$

the relative acceleration can be evaluated by means of

$$\boldsymbol{a}(t, \theta) = \boldsymbol{f_2}(\boldsymbol{x_h}(t), \boldsymbol{v_h}(t)) - \boldsymbol{f_2}(\boldsymbol{x_h}(t) + \boldsymbol{s}(\theta), \boldsymbol{v_h}(t)), \tag{16}$$

whose scalar product with $\boldsymbol{s}(\theta)$ will be the desired relative radial acceleration for each angle θ. In this manner, we denote by θ^* the angle at which the scalar product between $\boldsymbol{a}(t, \theta^*)$ and $\boldsymbol{s}(\theta^*)$ is equal to zero and, therefore, it will give us the relative position vector $\boldsymbol{r}$ that belongs to ZRRAL.

Now, we will show how to estimate the cost to maintain spacecraft in formation using the concept of residual acceleration. This concept can be used not only if the formation follows the direction of ZRRAL but for any rigid configuration.

3.1. Residual acceleration and cost estimate to maintain a spacecraft in a formation

Given a certain nominal trajectory $X_h(t)$ around L_4, suppose that a spacecraft follows an artificial trajectory around it, i.e. there exists a continuous effort (control) applied on it necessary to maintain that trajectory. Denote by $\boldsymbol{r_a}(t)$ the relative position at time t. If there is no continuous effort applied on the spacecraft, then the function $\mathbf{r_a}(t)$ will satisfy Eq. (11). However, if a control is applied on the spacecraft, there is a residual acceleration as a consequence of the

maneuvers applied on it. In this manner, denoting by $\mathbf{R_a}$ the residual acceleration, it can be computed using Eq. (11):

$$\boldsymbol{R_a} = \ddot{\boldsymbol{r}}_a - (F\boldsymbol{r_a} + J\dot{\boldsymbol{r}}_a). \tag{17}$$

Therefore, the cost estimate to maintain the spacecraft on an artificial trajectory until a time T is simply:

$$\Delta V = \left\| \int_0^T \boldsymbol{R_a}(t)dt \right\| \tag{18}$$

where $\| \ \|$ denotes the Euclidean norm.

In this simple manner, we can evaluate the cost estimate to maintain two or more satellites in formation along a periodic orbit around L_4.

4. Zero Relative Radial Acceleration Lines in a long and short period family

In this section we have determined the existence of Zero Relative Radial Acceleration Lines (ZRRAL) in periodic orbits around L_4. The existence of ZRRAL along any nominal trajectory is determined by the sign of the discriminant of the sub-matrix F in Eq. (13) which represents, in general, a quadratic form. The discriminant of F is defined by the following expression: $B^2 - 4AC$, where $A = \partial^2 U/\partial x^2$, $B = 2\partial^2 U/\partial x \partial y$, and $C = \partial^2 U/\partial y^2$. If the discriminant of F is negative at a certain point of the nominal trajectory, then, there is no region with Zero Relative Radial Acceleration (ZRRA). Otherwise, the ZRRA at this point is represented by two lines (in the planar case) (Lawrence, 1972; Barry, 2007).

First, we begin by computing the value of the discriminant of the sub-matrix F associated to points $X_h(t)$ in two periodic orbits close enough to L_4, as shown in Fig. 2. Their period is 92 days (long period, Fig. 2(a)) and 28 days (short period, Fig. 2(b)). These two orbits, as well as all of the periodic orbits shown in this section, are seen with respect to a non-dimensional coordinate system

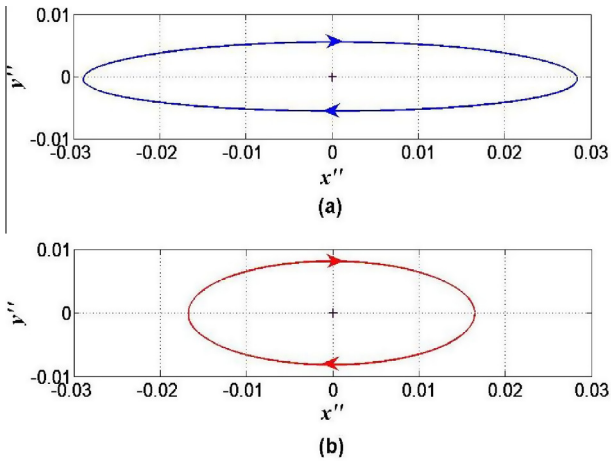

Fig. 2. Elliptic orbits centered at L_4 of (a) 92 days and (b) 28 days period. They correspond to the well known families of long and short period orbits about L_4 in the CRTBP.

x'', y'' rotated 29.7° clockwise about the equilibrium point L_4 (Szebehely, 1967).

As we can see in Fig. 3, the sign of the discriminant in both trajectories are negative for every point $X_h(t)$, meaning that there are no regions with ZRRA along these specific periodic orbits.

The previous fact can be verified when we compute numerically the ZRRA at some points on these periodic orbits. Thus considering a sphere of radius s equal to 1 km, the first row of Fig. 4 shows the scalar product between the relative acceleration $\boldsymbol{a}(t,\theta)$ and vector $\boldsymbol{s}(\theta)$ as a function of angle θ at three different points $X_h(t)$ along the long period orbit, where $t = 22$, 45 and 68 days. Similarly, the second row of Fig. 4 shows the scalar product at three different points $X_h(t)$ along the short period orbit, where $t = 7$, 14 and 22 days.

Now, if we make a zoom around the maximum point of each dot product function shown in Fig. 4, the scalar product function between the relative acceleration and relative position vectors never crosses the horizontal axis for any angle θ at each of these three points $X_h(t)$, as we can see in Fig. 5. Therefore the radial component of the relative acceleration $\boldsymbol{a}(t,\theta)$ is different from zero for any angle θ at each one of these three points. It is important to comment that the dot product computed in this work is dimensionless because we are using the normalized system. If we want to obtain the scalar product in physical units, i.e. meters and seconds (time and length), we have to multiply the previous results by a factor of 1.0469×10^6 m/s^2. In any case, the qualitative behavior of the scalar product function shown in Fig. 4 will remain the same. Additionally, from Fig. 4 we can see that the scalar product function is periodic (period equal to 180°) and has two maxima and two minima. Thus, the radial component of the relative acceleration $\boldsymbol{a}(t,\theta)$ has also two maxima and two minima at the same previous optimal values of θ. In Fig. 6 we show the angle θ for each point $X_h(t)$ where the relative radial acceleration has a maximum and a minimum value along the long (first row) and short (second row) period orbits shown in Fig. 2.

From this first case, we could state that there are no regions with ZRRA along the periodic orbits that are close enough to L_4. The next step, therefore, is to explore the existence of regions with ZRRA along periodic orbits that are far from L_4.

Fig. 7 shows two periodic orbits around L_4, which belong to the long (92 days) and short (21 days) period families, in the non-dimensional coordinate system x'', y''. Both are much larger, i.e. the amplitude is larger when compared to the periodic orbits shown in Fig. 2.

Similarly, Fig. 8(a) and (b) show the value of the discriminant of the sub-matrix F associated to the points $X_h(t)$ along the long and short period orbits shown in Fig. 7. Unlike the previous case, the sign of the discriminant in both trajectories are negative and positive, this means that although there do not exist regions with ZRRA at certain points along the periodic orbits, there exist some

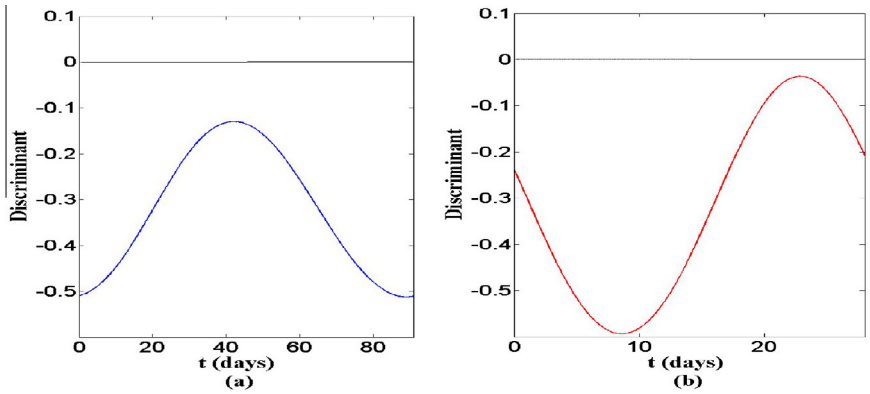

Fig. 3. Discriminant of the sub-matrix F associated to the points $X_h(t)$ in the (a) long and (b) short period orbits shown in Fig. 2.

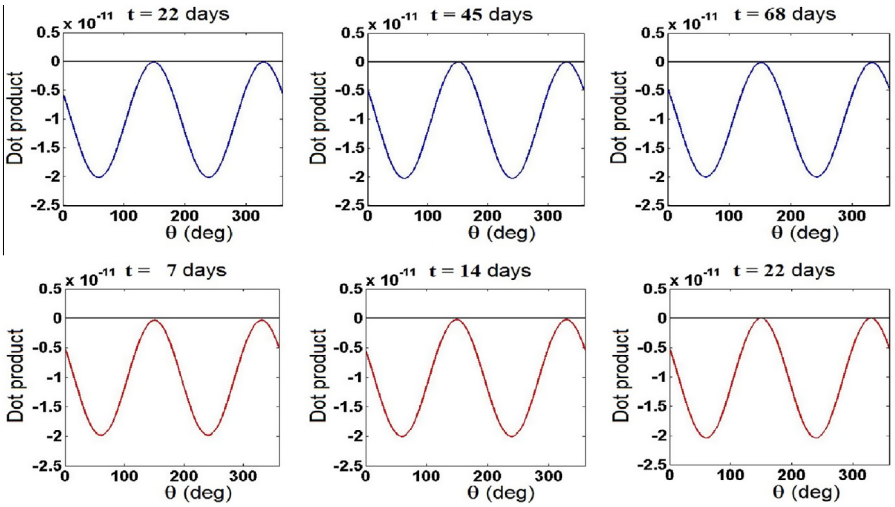

Fig. 4. Scalar product between the relative acceleration $\boldsymbol{a}(t,\theta)$ and vector $\boldsymbol{s}(\theta)$ as a function of angle θ at three different points $X_h(t)$ along the long (first row) and short (second row) period orbits shown in Fig. 2.

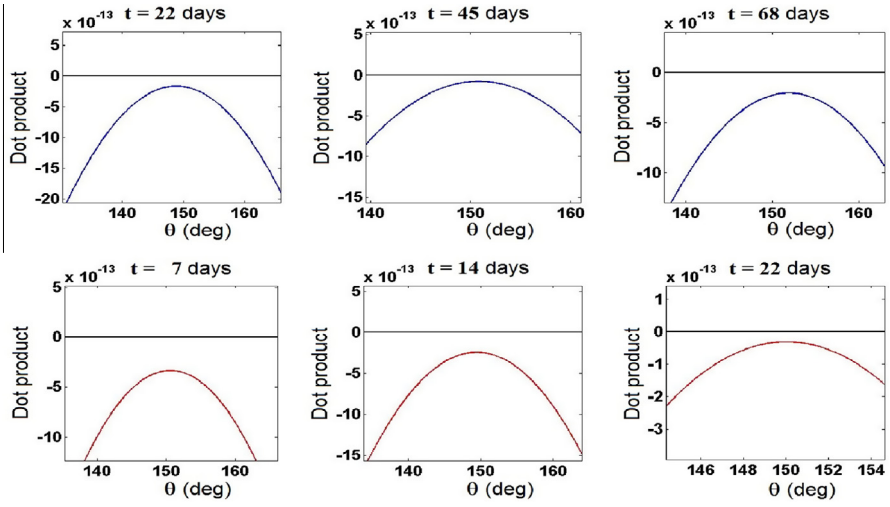

Fig. 5. Scalar product between the relative acceleration $\boldsymbol{a}(t,\theta)$ and vector $\boldsymbol{s}(\theta)$ as a function of angle θ at three different points $X_h(t)$ along the long (first row) and short (second row) period orbits shown in Fig. 2.

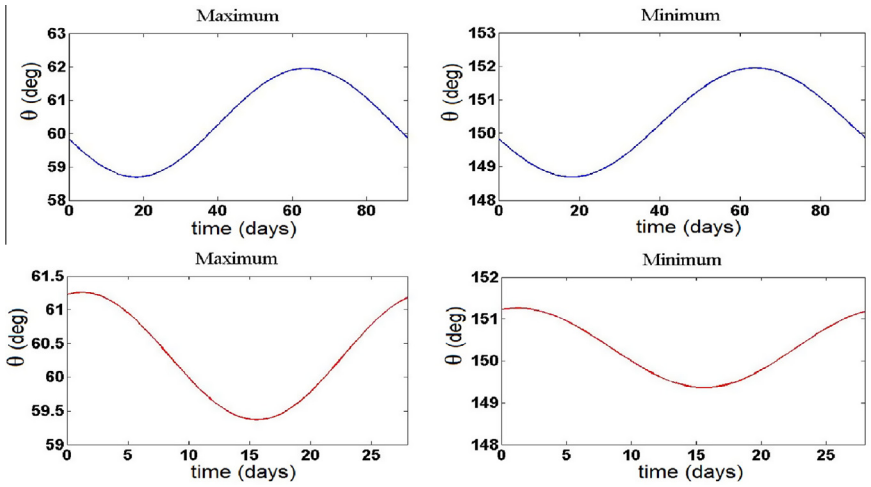

Fig. 6. Angle θ for each point $X_h(t)$ where the relative radial acceleration has a maximum and minimum value on the long (first row) and short (second row) period orbits shown in Fig. 2.

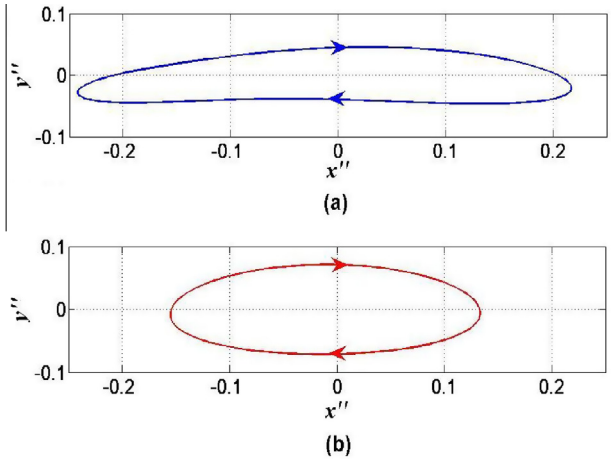

Fig. 7. (a) Long and (b) short period orbits around L_4.

parts along these periodic orbits where the radial component of the relative acceleration is equal to zero. This fact can also be seen if we consider a sphere of radius s equal to 1 km as shown in Fig. 9 and we compute numerically the ZRRA at three different points $X_h(t)$ along the previous periodic orbits.

The qualitative behavior of the scalar product function is very similar for all the values of t where there appear two maxima and two minima. However, there is a set of points in these trajectories where the radial component of the function $\boldsymbol{a}(t,\theta)$ is zero with vertex at $\boldsymbol{x_h}(t)$ for two different values of θ, which we have denoted by θ^* and θ^{**} (where $\theta^* \leqslant \theta^{**}$). Note that since the scalar product function is periodic with respect to θ, the other two zeros represent the same situation. Fig. 10(a) and (b) show the function θ associated to point $X_h(t)$, such that, the relative radial acceleration is maximum for all values of t along the long and short period orbits shown in Fig. 7, respectively. Similarly, Fig. 11 shows the function θ for the values where the relative radial acceleration is minimum or zero for the long (first row) and short (second row) period orbits. As we can see in Fig. 11, when we only compute the values of θ where the scalar product function has a minimum, the function θ is smooth. But, when we compute the points where the scalar product function has a minimum or a zero, there are two points where this function is not

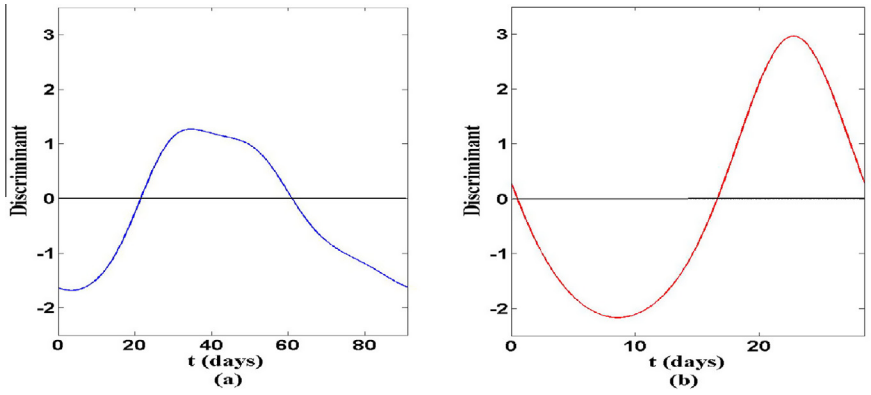

Fig. 8. Discriminant of the sub-matrix F associated to the points in the (a) long and (b) short period orbits shown in Fig. 7.

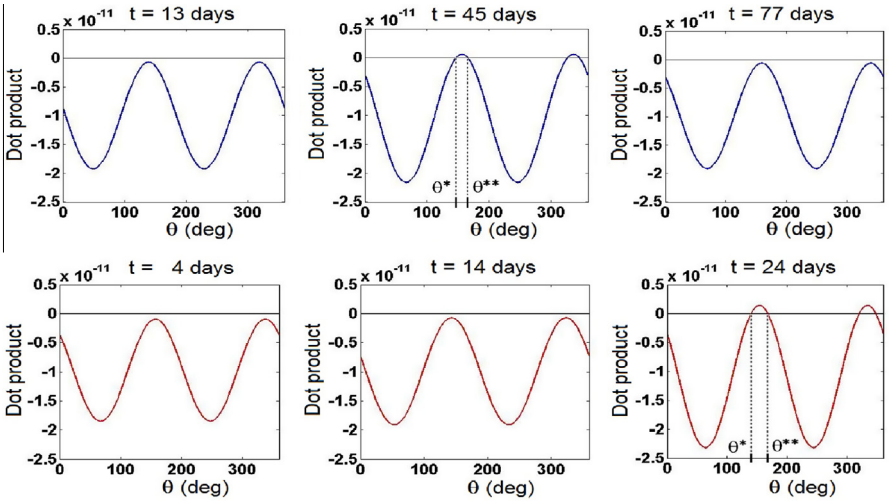

Fig. 9. Scalar product between the relative acceleration $\mathbf{a}(t,\theta)$ and vector $\mathbf{s}(\theta)$ as a function of angle θ at three different points $X_h(t)$ on the long (first row) and short (second row) period orbits shown in Fig. 7.

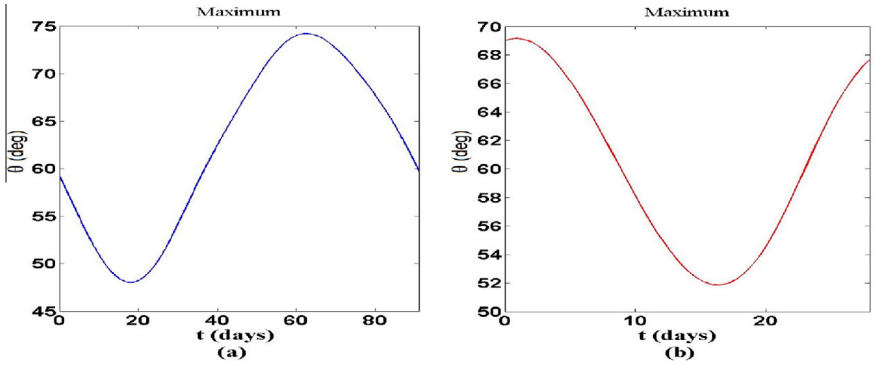

Fig. 10. Angle θ for each point $X_h(t)$ where the relative radial acceleration has a maximum value for the (a) long and (b) short period orbits shown in Fig. 7.

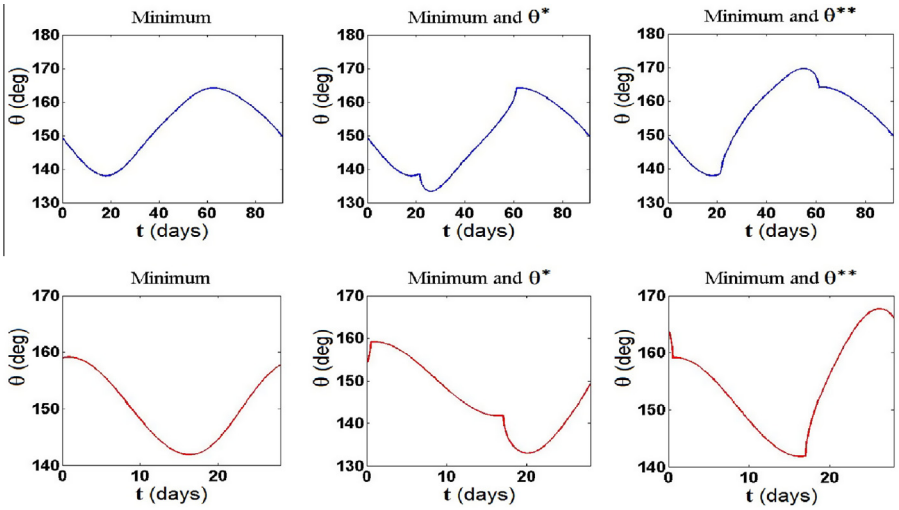

Fig. 11. Angle θ for each point $X_h(t)$ where the relative radial acceleration has a minimum or zero value for the long (first row) and short (second row) period orbits shown in Fig. 7.

smooth. This fact implies a higher cost to maintain a rigid constellation as will be shown later.

Finally, Fig. 12(a) and (b) show the family of long and short period around L_4. Similarly, we compute the discriminant of the sub-matrix F along each periodic orbit as shown in Fig. 13. This result supports a fact that was previously shown. When their amplitude is small enough, there are no ZRRAL. However, when their amplitude is large enough, ZRRA regions exist and their size increases with the amplitude.

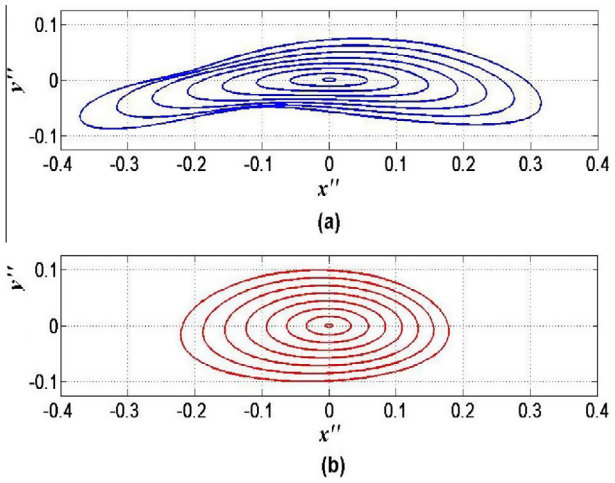

Fig. 12. (a) Long and (b) short period families around L_4. Their periods are about 92 days and 28 days, respectively.

We have computed the value of θ for every point $X_h(t)$ along each orbit that belongs to the long and short period families where the radial component acceleration is maximum, minimum or zero (in the cases where the discriminant is positive). Fig. 14(a) and (b) show the value of θ such that the radial acceleration component is maximum for the long and short period families, respectively.

In the same way, for periodic orbits that are large enough, the function θ has a minimum and two zeros. Fig. 15 shows the value of θ such that the radial acceleration component is minimum or zero (denoted by θ^* and θ^{**}) for the long (first row) and short (second row) period families, respectively.

5. Cost estimate to maintain a spacecraft on the regions of zero, minimum and maximum relative radial accelerations

Considering a radius s equal to 1 km, Table 1 shows the cost estimate per year to maintain the spacecraft when the artificial trajectory follows the direction where the relative radial acceleration component is maximum (see left column

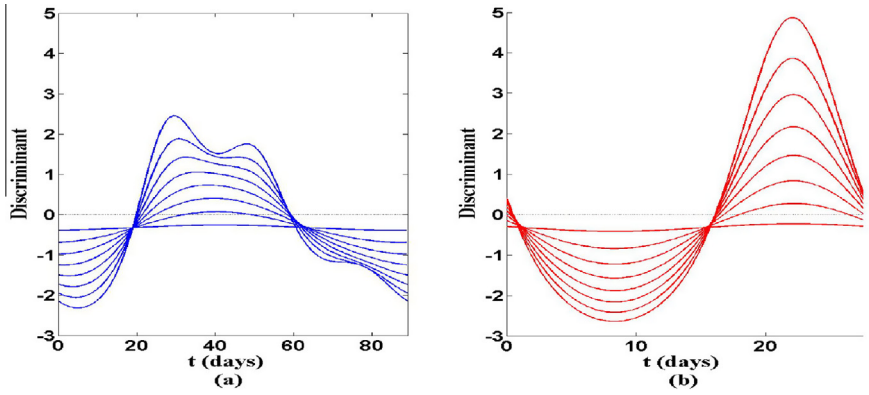

Fig. 13. Discriminant of the sub-matrix F associated to the points in the (a) long and (b) short period families shown in Fig. 12.

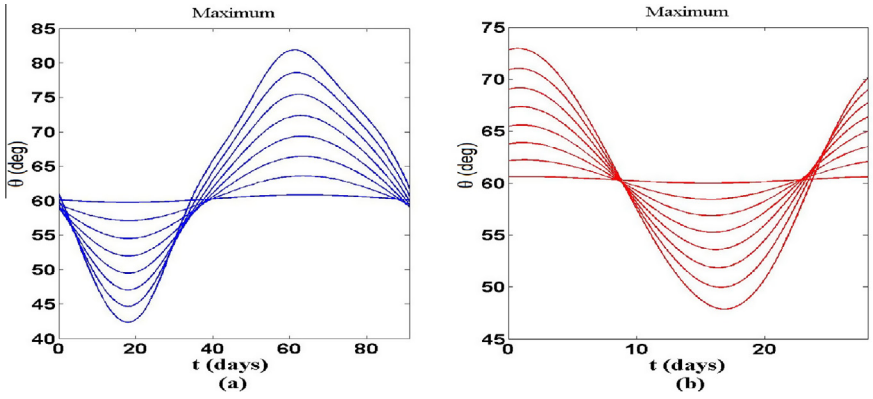

Fig. 14. Angle θ for each point $X_h(t)$ where the relative radial acceleration has a maximum value for the (a) long and (b) short period families shown in Fig. 12.

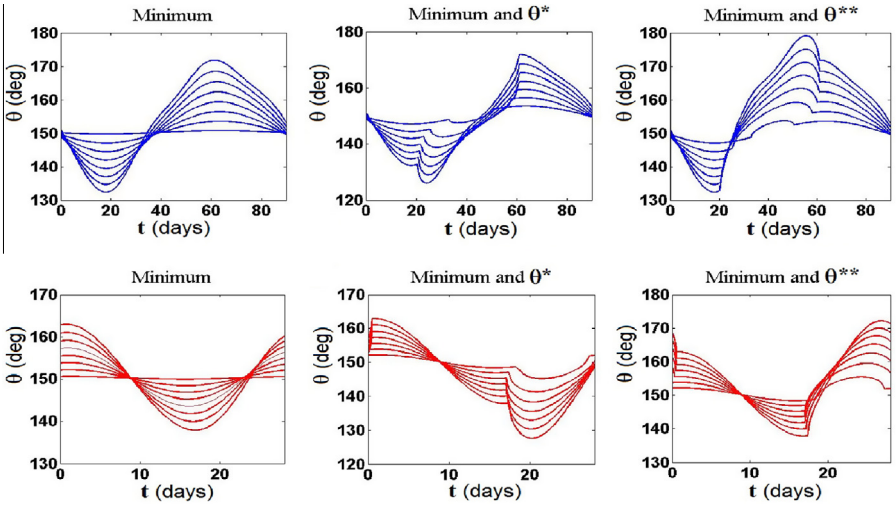

Fig. 15. Angle θ for each point $X_h(t)$ where the relative radial acceleration has a minimum or zero value for the long (first row) and short (second row) period families shown in Fig. 12.

Table 1
Cost estimate per year to maintain a spacecraft considering a radius of 1 km and following the direction where the relative radial acceleration component is maximum and minimum with respect to the periodic orbits shown in Fig. 2.

Orbital period	Cost estimate Maximum radial acceleration (m/s)	Cost estimate Minimum radial acceleration (m/s)
Long	6.5777×10^{-1}	6.0422×10^{-3}
Short	6.2989×10^{-1}	6.1713×10^{-3}

in Fig. 6) and minimum (see right column in Fig. 6) with respect to the periodic orbits shown in Fig. 2. It was found that there exists a linear relation between the distance from $X_h(t)$ and the cost estimate when the radius s is small enough. Additionally, the costs between the long and short period orbits are almost equal.

Now, suppose a spacecraft placed in an artificial trajectory around the periodic orbits shown in Fig. 7. Similarly, considering a radius s equal to 1 km, Table 2 shows the cost estimate per year to maintain the spacecraft following the direction where the relative radial acceleration component is maximum (see Fig. 10), minimum and zero (see Fig. 11). Similarly, there exists a linear relation between the cost and the radius of the artificial trajectory when s is small enough.

Note that the cost estimate to maintain the spacecraft, on the direction when the relative radial acceleration is minimum but not zero, is much less (almost ten times) when compared to the cost to maintain the spacecraft on the direction where the relative radial acceleration is minimum or zero (see Table 2). This fact can be understood if we compute the components x and y of the relative position, velocity and acceleration vectors described in Eq. (17). For example, Fig. 16 shows the components x (left column) and y (right column) of the relative position $\boldsymbol{r_a}$ (first row), relative velocity $\dot{\boldsymbol{r}}_a$ (second row) and relative acceleration $\ddot{\boldsymbol{r}}_a$ (third row) of the artificial trajectory following the direction where the relative radial acceleration component is minimum on the long period orbit shown in Fig. 7. Similarly, Fig. 17 shows the components of these vectors when the relative radial acceleration component is minimum or zero on the long period orbit shown in Fig. 7. Note that in Fig. 16 the two components for $\boldsymbol{r_a}$, $\dot{\mathbf{i}}_a$, $\ddot{\boldsymbol{r}}_a$, are smooth functions. However, in Fig. 17 we can see that the components for each vector are not. In fact, the function $\boldsymbol{r_a}$ is not smooth at time t when the regions of ZRRA appear and disappear (see Fig. 11). Therefore, we see two big jumps in the functions $\dot{\boldsymbol{r}}_a$ and $\ddot{\boldsymbol{r}}_a$ at these two points. The function $\boldsymbol{R_a}$ is bigger in the region where the ZRRA exists as shown in Fig. 18. As a consequence, the cost estimate ΔV will be less than that when the artificial trajectory follows the

Table 2
Cost estimate per year to maintain a spacecraft considering a radius of 1 km following the direction where the relative radial acceleration component is maximum, minimum and zero with respect to the periodic orbits shown in Fig. 7.

Orbital period	Cost estimate Maximum radial acceleration (m/s)	Cost estimate Minimum radial acceleration (m/s)	Cost estimate Minimum and zero (θ^*) radial acceleration (m/s)	Cost estimate Minimum and zero (θ^{**}) radial acceleration (m/s)
Long	6.6074×10^{-1}	7.0033×10^{-3}	6.4182×10^{-2}	6.5106×10^{-2}
Short	6.3015×10^{-1}	2.1255×10^{-2}	1.3563×10^{-1}	1.3635×10^{-1}

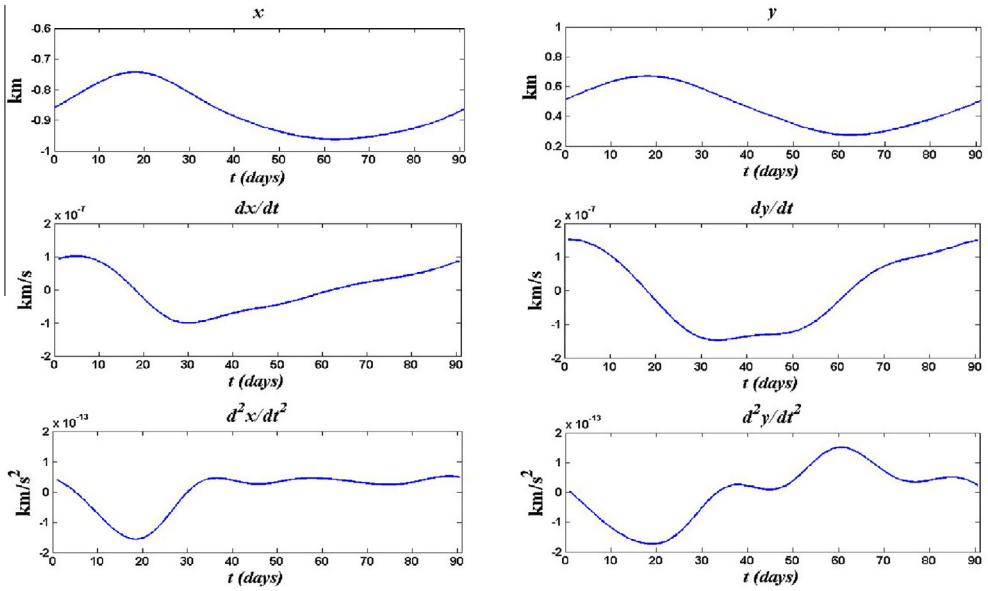

Fig. 16. Components x (right column) and y (left column) of relative position $\boldsymbol{r}_a$ (first row), relative velocity $\dot{\boldsymbol{r}}_a$ (second row) and relative acceleration $\ddot{\boldsymbol{r}}_a$ (third row) of the artificial trajectory that follows the direction where the relative radial acceleration component is minimum in the long period orbit shown in Fig. 7.

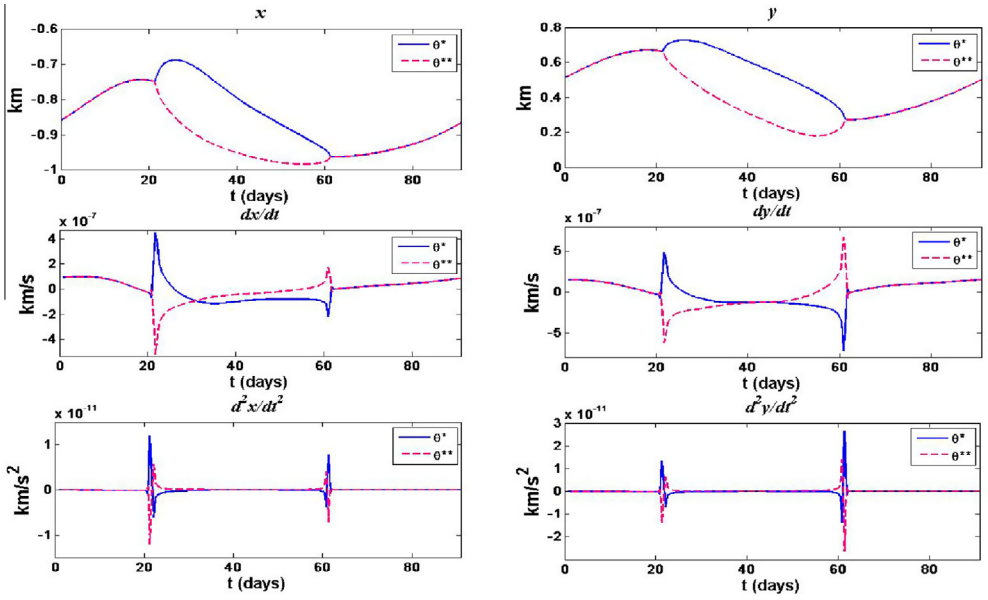

Fig. 17. Components x (right column) and y (left column) of relative position $\boldsymbol{r}_a$ (first row), relative velocity $\dot{\boldsymbol{r}}_a$ (second row) and relative acceleration $\ddot{\boldsymbol{r}}_a$ (third row) of the artificial trajectory that follows the direction where the radial acceleration component is minimum or zero in the long period orbit shown in Fig. 7.

direction where the relative radial acceleration is minimum but not zero.

Similarly, suppose that we denote the family of periodic orbits as shown in Fig. 19, where Orbit 1 denotes the smallest one and Orbit 8 denotes the largest one. Considering a radius equal to 1 km, Tables 3 and 4 show the cost estimate per year to maintain a spacecraft in each orbit of the long and short period family, respectively, following the direction where the relative radial acceleration component is maximum, minimum and zero. Additionally, the magnitude of the segment where each orbit intersects the positive x-axis is also shown. This quantity is useful to represent the amplitude of each orbit. As can be seen in Tables 3 and 4, the cost estimate following the direction where the radial acceleration component is maximum practically remains constant, i.e., it does not depend on the amplitude of the periodic orbits. On the other hand, following the direction where the radial acceleration component is minimum or zero, the cost to maintain a spacecraft increases with the amplitude.

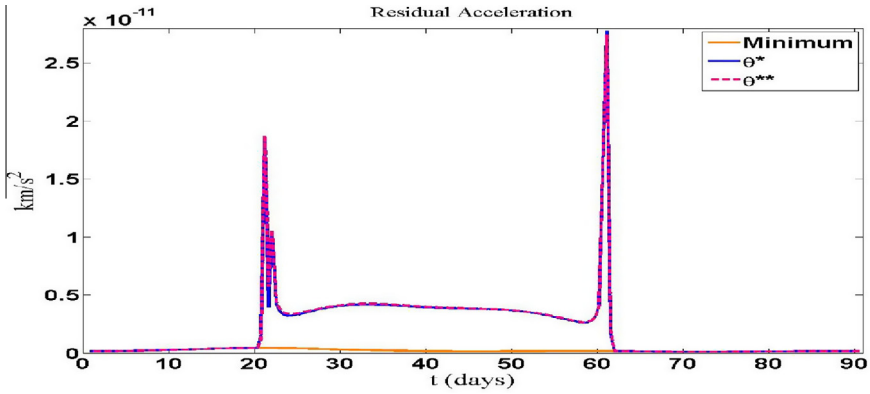

Fig. 18. Residual acceleration of the artificial trajectory that follows the direction where the relative radial acceleration component is minimum or zero with respect to the long period orbit shown in Fig. 7.

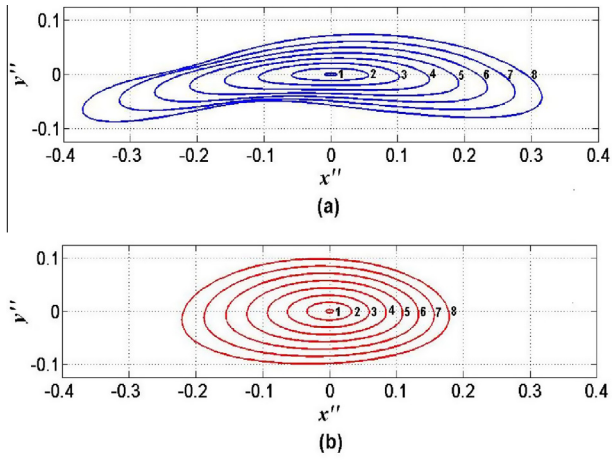

Fig. 19. Family of periodic orbits shown in Fig. 12, where Orbit 1 denotes the smallest one and Orbit 8 denotes the largest one.

Finally, it is important to comment that although all simulations made in this section show that the cost estimate to maintain a satellite in the region of maximum relative radial acceleration is almost ten times higher than the cost estimate to maintain it in the region of minimum relative radial acceleration, the values estimated are very low (the residual acceleration is order of 10^{-8} m/s^2), such small continuous acceleration to control the relative position of a satellite can not be implemented in practical engineering applications. In this manner, effects of the Moon's eccentricity and the Sun must be considered in the dynamical model to correct the cost estimate to maintain the formation. However, as will be shown in Section 7, the significance of the ZRRAL is not only in minimizing the cost of correction maneuvers but also in determining the initial conditions of the SFF that minimize the drift of the formation. In practice, it is difficult to find initial conditions that eliminate inter-spacecraft drift because of perturbations. By contrast, the initial conditions can be picked up in such a way minimizing the need for corrective action.

6. Cost estimate to maintain a formation on a rigid configuration

In the previous section, we studied the cost estimate of configurations that follows the direction where the relative radial acceleration is maximum, minimum or zero. However, many space missions (e.g., interferometry missions) require fixed relative positions and specific geometric templates. Therefore, in this section we study the case when the geometry of the configuration remains constant, i.e. the angle θ is fixed (see Fig. 24).

Table 3
Cost estimate per year to maintain a spacecraft in each orbit of the long period family shown in Fig. 19 considering a radius equal to 1 km and following the direction where the relative radial acceleration component is maximum, minimum and zero.

Periodic orbit	Amplitude (km)	Cost estimate Maximum radial acceleration (m/s)	Cost estimate Minimum radial acceleration (m/s)	Cost estimate Minimum and zero (θ^*) radial acceleration (m/s)	Cost estimate Minimum and zero (θ^{**}) radial acceleration (m/s)
1	3.6614×10^3	6.5750×10^{-1}	6.0286×10^{-3}		
2	2.1526×10^4	6.5792×10^{-1}	6.0881×10^{-3}	1.5004×10^{-2}	1.5062×10^{-2}
3	3.8517×10^4	6.5850×10^{-1}	6.2313×10^{-3}	3.3591×10^{-2}	3.3850×10^{-2}
4	5.4585×10^4	6.5925×10^{-1}	6.4562×10^{-3}	4.5180×10^{-2}	4.5567×10^{-2}
5	6.9807×10^4	6.6014×10^{-1}	6.7676×10^{-3}	5.5834×10^{-2}	5.6401×10^{-2}
6	8.4300×10^4	6.6116×10^{-1}	7.1855×10^{-3}	7.3302×10^{-2}	7.4046×10^{-2}
7	9.8100×10^4	6.6230×10^{-1}	7.7586×10^{-3}	8.3866×10^{-2}	8.4787×10^{-2}
8	1.1171×10^5	6.6360×10^{-1}	8.6312×10^{-3}	8.7558×10^{-2}	8.8503×10^{-2}

Table 4
Cost estimate per year to maintain a spacecraft in each orbit of the short period family shown in Fig. 19 considering a radius equal to 1 km and following the direction where the relative radial acceleration component is maximum, minimum and zero.

Periodic orbit	Amplitude (km)	Cost estimate Maximum radial acceleration (m/s)	Cost estimate Minimum radial acceleration (m/s)	Cost estimate Minimum and zero (θ^*) radial acceleration (m/s)	Cost estimate Minimum and zero (θ^{**}) radial acceleration (m/s)
1	2.1238×10^3	6.4023×10^{-1}	5.9153×10^{-3}		
2	1.2570×10^4	6.4013×10^{-1}	7.4009×10^{-3}	6.4286×10^{-2}	6.4920×10^{-2}
3	2.2641×10^4	6.4025×10^{-1}	1.0242×10^{-2}	9.1027×10^{-2}	9.1375×10^{-2}
4	3.2443×10^4	6.4054×10^{-1}	1.3850×10^{-2}	9.9301×10^{-2}	1.0013×10^{-1}
5	4.1900×10^4	6.4092×10^{-1}	1.7736×10^{-2}	1.2289×10^{-1}	1.2372×10^{-1}
6	5.1048×10^4	6.4137×10^{-1}	2.1740×10^{-2}	1.3883×10^{-1}	1.3987×10^{-1}
7	5.9851×10^4	6.4189×10^{-1}	2.5826×10^{-2}	1.4365×10^{-1}	1.4685×10^{-1}
8	6.8347×10^4	6.4255×10^{-1}	2.9996×10^{-2}	1.8064×10^{-1}	1.8140×10^{-1}

Considering a radius of 1 km, Fig. 20(a) and (b) show the cost estimate per year to maintain a spacecraft in each orbit of the long and short period family shown in Fig. 19, keeping the angle θ constant.

Note that the cost function in Fig. 20 has a period of 180°. Additionally, the function has two maxima at $\theta \approx 60°$ and 240°, and two minima at $\theta \approx 150°$ and 330°. These values practically coincide with the direction in which the relative radial acceleration component is maximum and minimum (see Fig. 6) for the periodic orbits shown in Fig. 2. In fact, the costs compared with these cases are similar.

Now, we will study a triangular geometry around the periodic orbits shown in Figs. 2 and 7. In this configuration we consider a formation of three satellites such that their positions and distances with respect to periodic orbit are fixed and form an equilateral triangle. There are three cases we have analyzed in this formation as shown in Fig. 21:

(a) The periodic solution $X_h(t)$ remains in the center of the equilateral triangle.
(b) The periodic solution $X_h(t)$ remains in the middle of one of the sides.
(c) One of the satellites remains on the periodic solution $X_h(t)$.

In these three cases, the orientation of the formation is defined by the angle θ, which denotes the direction of the relative position of satellite 1. Once the angle θ is fixed, the other angles that define the relative positions of satellites 2 and 3 are easily computed by elementary geometry. The cost estimate to maintain the formation is simply the sum of the cost estimates to maintain each satellite in the selected position. Fig. 22(a) and (b) show the cost function of the triangular formation along the long and short period orbits around L_4 shown in Fig. 2, for $0° \leqslant \theta \leqslant 180°$ (the cost function has a period of 180°) and a time $T = 1$ year.

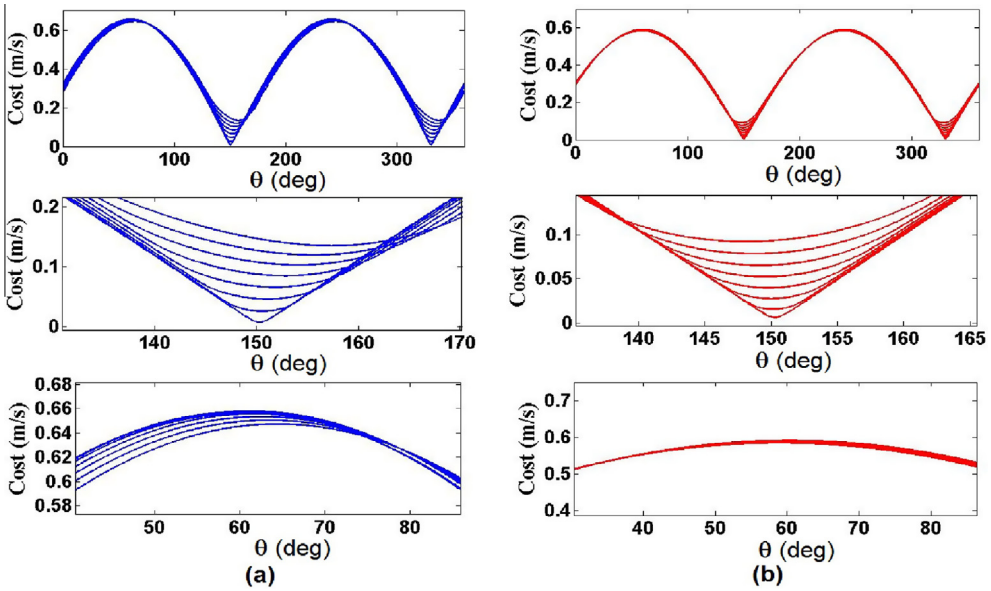

Fig. 20. Cost estimate per year to maintain a spacecraft in the long (a) and short (b) period family shown in Fig. 12 fixing the angle θ and considering a radius of 1 km.

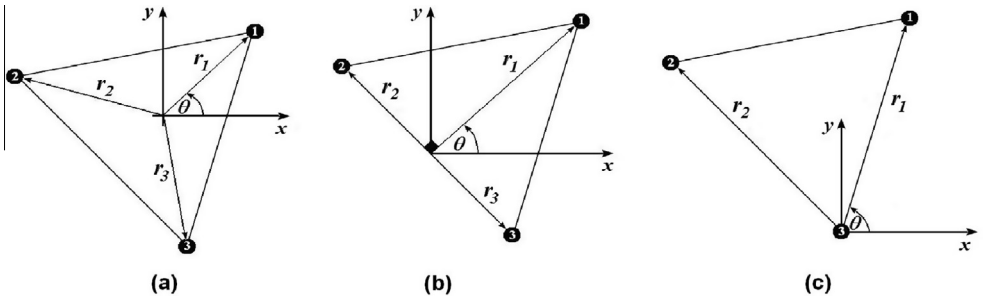

Fig. 21. Formation of three satellites such that their positions and distances in the periodic orbit are fixed and form an equilateral triangle.

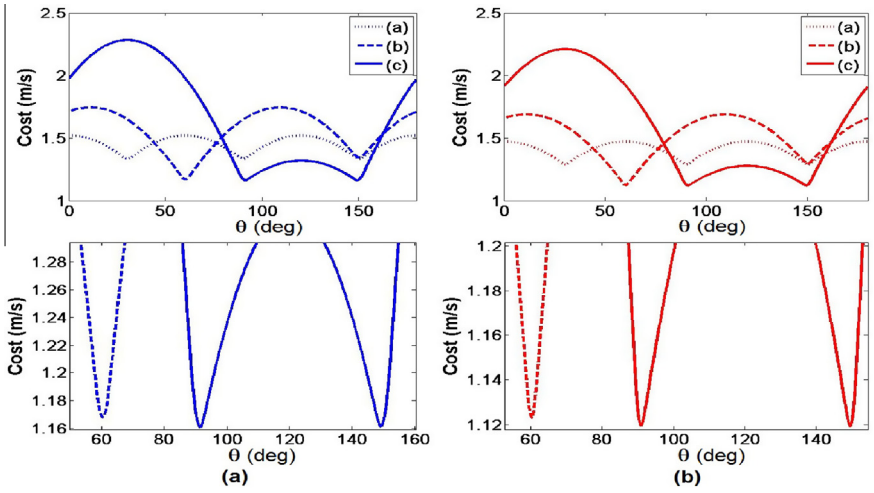

Fig. 22. Cost estimate per year to maintain a formation of three satellites considering configurations (a), (b) and (c) in the long and short period orbits shown in Fig. 2.

The length of the side of the equilateral triangle is equal to 2 km. As we can see in Fig. 22, for the long and short period orbits, the minimum cost is obtained when the formation follows the configuration (c) for $\theta = 90^\circ$ and $\theta = 150^\circ$. However, we note that the cost of configuration (b) is almost the same when $\theta = 60^\circ$. Therefore, it can be said that the minimum cost is obtained when the formation follows the configuration (b) and (c) and one of the satellites is located along the direction of $\theta = 150^\circ$.

Finally, Fig. 23(a) and (b) show the cost estimate function of the triangular formation on the long and short period orbits around L_4 shown in Fig. 7. The results show that

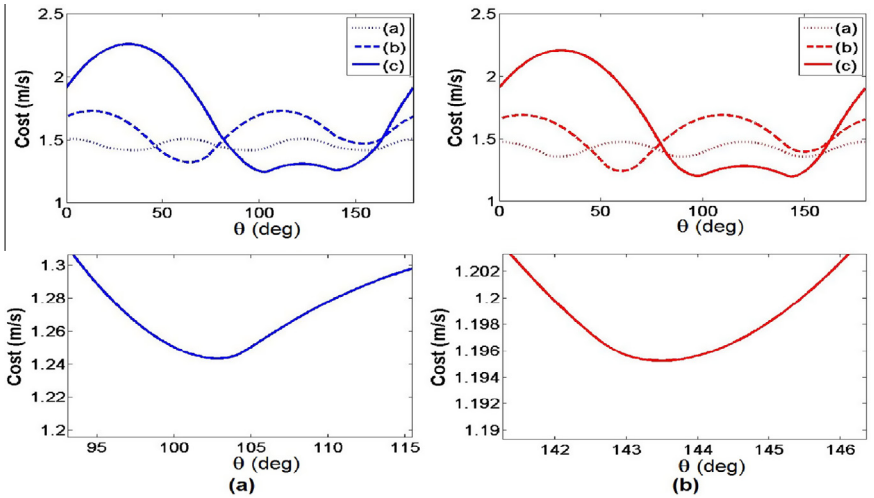

Fig. 23. Cost estimate per year to maintain a formation of three satellites considering configurations (a), (b) and (c) in the long and short period orbits shown in Fig. 7.

the minimum cost estimate is obtained when the formation follows the configuration (c) for $\theta = 103^\circ$ and $\theta = 143^\circ$ for the long and short period orbits, respectively. Additionally, it is interesting to remark that the configuration (c) is not only the case where we obtain the minimum cost, but also the maximum cost depending of the choice of this angle. Similarly, effects of the Moon's eccentricity and the Sun are necessary to correct the cost to maintain each rigid configuration.

7. Dynamical behavior of different classes of solutions

Using polar coordinates, let us define an initial condition

$$X(0) = (\boldsymbol{x_h}(0) + (r(0)\cos\theta(0), r(0)\sin\theta(0)), \boldsymbol{v_h}(0)), \quad (19)$$

as illustrated in Fig. 24. In this last section, we want to study the dynamical behavior of the distance, denoted by $d(X_h(t), X(t))$, between the spacecraft and the periodic orbit at each time t using the nonlinear model, i.e. without linearizing the vector field $\Delta X(t) = X(t) - X_h(t)$. First, Fig. 25 shows the value of the maximum separation during 2 years for $0^\circ \leqslant \theta(0) \leqslant 360^\circ$ and $r(0) = 1,\ 2$ km along the long period orbit shown in Fig. 2. Similarly, Fig. 26 shows the value of the maximum separation during 2 years along the short period orbit shown in Fig. 2. We have numerically integrated these two initial conditions and the best and worst cases occur when $\theta(0) = 150^\circ$ and $\theta(0) = 60^\circ$, respectively. This fact does not depend on the initial condition $X_h(0)$. Therefore, the distance will be computed when $\theta(0) = 150^\circ$ and $\theta(0) = 60^\circ$ to compare the difference between the quantitative behavior of $d(X_h(t), X(t))$.

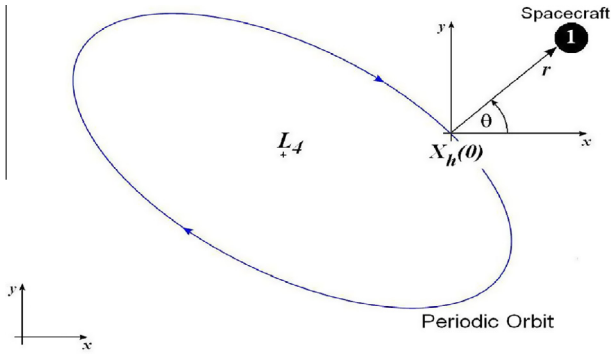

Fig. 24. Illustration of the relative position of a spacecraft around a periodic orbit of L_4.

For the first case, we have taken four relative initial vectors $\boldsymbol{r_1}(0)$, $\boldsymbol{r_2}(0)$, $\boldsymbol{r_3}(0)$, and $\boldsymbol{r_4}(0)$ along the direction of $\theta(0) = 150^\circ$ associated to the initial condition $X_h(0)$ of the periodic orbit around L_4 (see Fig. 24). The vectors have been distributed symmetrically with respect to $X_h(0)$: $\boldsymbol{r_1}(0)$ and $\boldsymbol{r_3}(0)$ being at an initial distance of 1 km from $X_h(0)$ and, $\boldsymbol{r_2}(0)$ and $\boldsymbol{r_4}(0)$ being at an initial distance of 2 km. We have integrated these trajectories during three years and the results are shown in the first row of Fig. 27. As we can see, the maximum deviation from the starting separations is less than 1.5 km for the orbits with initial vectors $\boldsymbol{r_i}(0)$. The distance $d(X_h(t), X_i(t))$ is a periodic function with period equal to 460 days. Additionally, there is no difference between the qualitative and quantitative behavior of the distance for the trajectories starting at the same distance from $X_h(0) : d(X_h(t), X_1(t)) \approx d(X_h(t), X_3(t))$ and $d(X_h(t), X_2(t)) \approx d(X_h(t), X_4(t))$.

Now, for the second case, we take four relative initial vectors $\boldsymbol{q_1}(0)$, $\boldsymbol{q_2}(0)$, $\boldsymbol{q_3}(0)$, and $\boldsymbol{q_4}(0)$ along the direction of $\theta(0) = 60^\circ$ corresponding also to the initial condition $X_h(0)$ of the periodic orbit around L_4, distributed in a similar fashion to the previous case. In the second row of

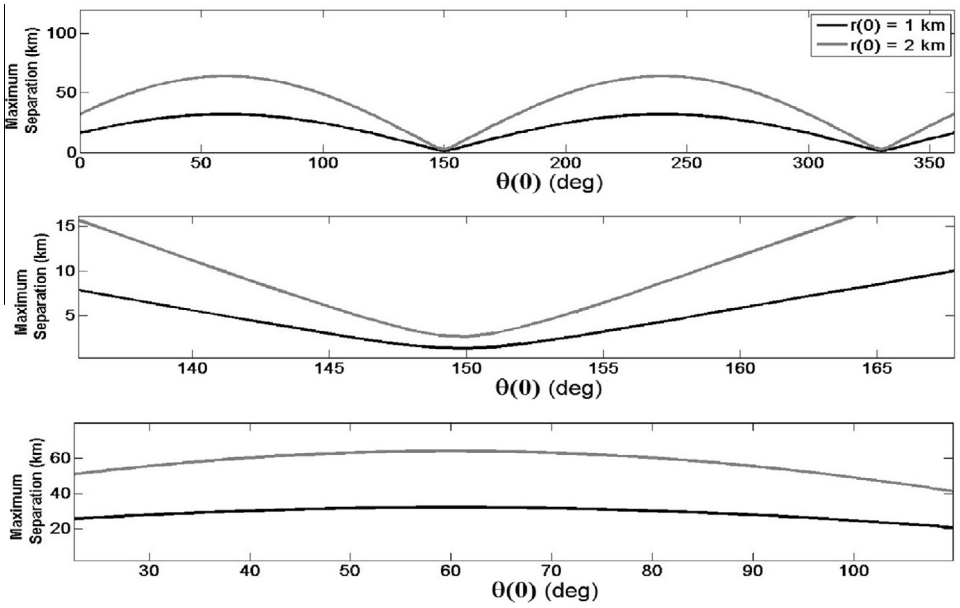

Fig. 25. Maximum separation (in km) during 2 years for $0^\circ \leqslant \theta(0) \leq 360^\circ$ and $r(0) = 1,\ 2$ km along the long period orbit shown in Fig. 2.

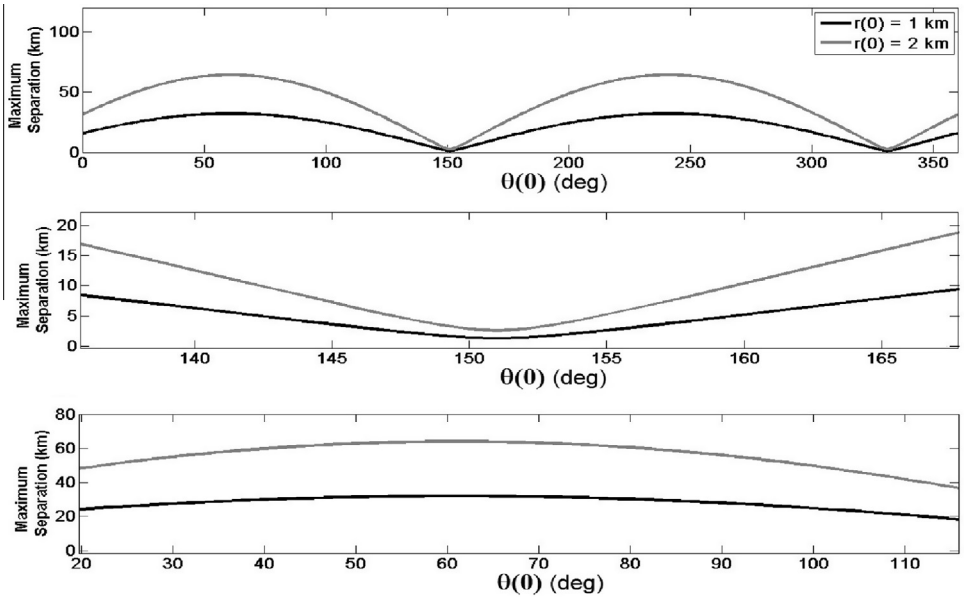

Fig. 26. Maximum separation (in km) during 2 years for $0^\circ \leqslant \theta(0) \leq 360^\circ$ and $r(0) = 1,\ 2$ km along the short period orbit shown in Fig. 2.

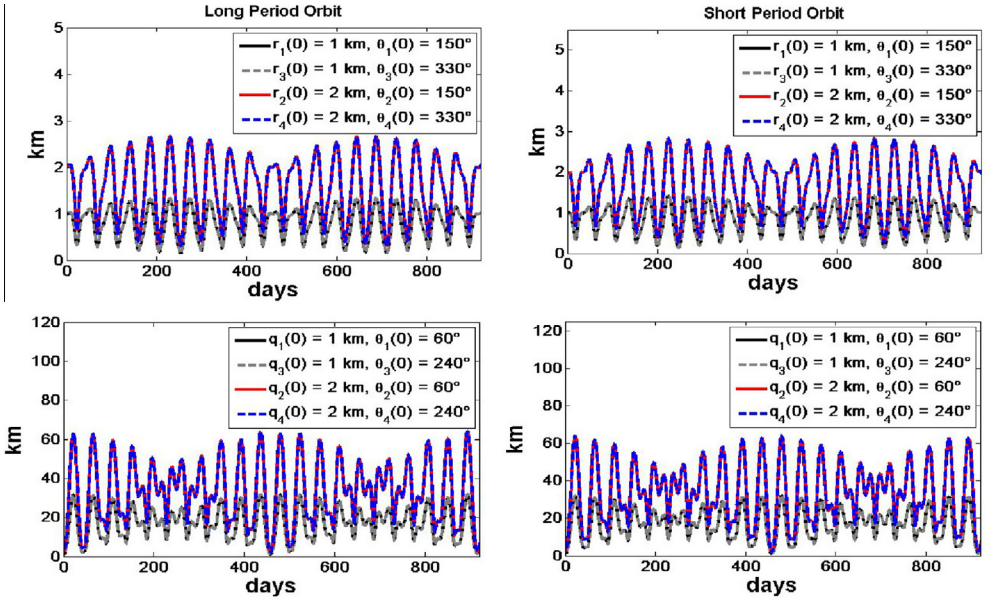

Fig. 27. Distance $d(X_h(t), X_i(t))$, between the trajectories of $\boldsymbol{r_1},\ \boldsymbol{r_2},\ \boldsymbol{r_3},\ \boldsymbol{r_4}$ (first row), and $\boldsymbol{q_1},\ \boldsymbol{q_2},\ \boldsymbol{q_3},\ \boldsymbol{q_4}$ (second row), and the long and short period orbits shown in Fig. 2.

Fig. 27 the results are shown for the distance $d(X_h(t), X_i(t))$. Now, although the qualitative behavior is also periodic (period equal to 460 days) and there is no difference between the qualitative and quantitative behavior of the distance for the trajectories starting at the same distance from $X_h(0)$, the deviations from the periodic orbit are larger (they increase by a factor of 40) than the ones obtained for the $\boldsymbol{r}_i(0)$ initial vectors taken along the direction of $\theta(0) = 150^\circ$.

The same study is made along the long and short period orbits shown in Fig. 7. The purpose is also to analyze the dynamical behavior of the distance for periodic orbits that are larger. In Fig. 28 it can be seen that the best position to minimize the deviation is along the direction of $\theta(0) = 149^\circ$ associated to the initial condition of the long period orbit. In the same way, the position that maximize the deviation is along the direction of $\theta(0) = 59^\circ$. Practically, the difference with respect to the previous results is only 1°. Similarly, Fig. 29 shows that the position to minimize and maximize the deviation is along the direction of $\theta(0) = 157^\circ$ and $\theta(0) = 67^\circ$, respectively, associated to the initial condition of the short period orbit. In this case, the difference with respect to the previous results is 7°.

Similarly, we take four relative initial vectors along the direction of minimum and maximum deviation corresponding also to the initial condition $X_h(0)$ of the periodic

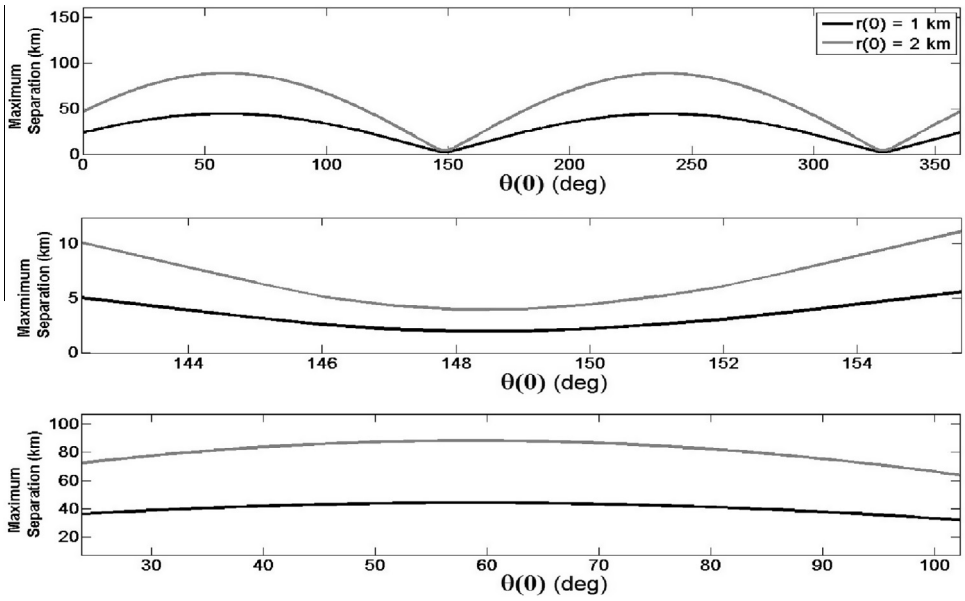

Fig. 28. Maximum separation (in km) during two years for $0^\circ \leqslant \theta(0) \leq 360^\circ$ and $r(0) = 1,\ 2$ km along the long period orbit shown in Fig. 7.

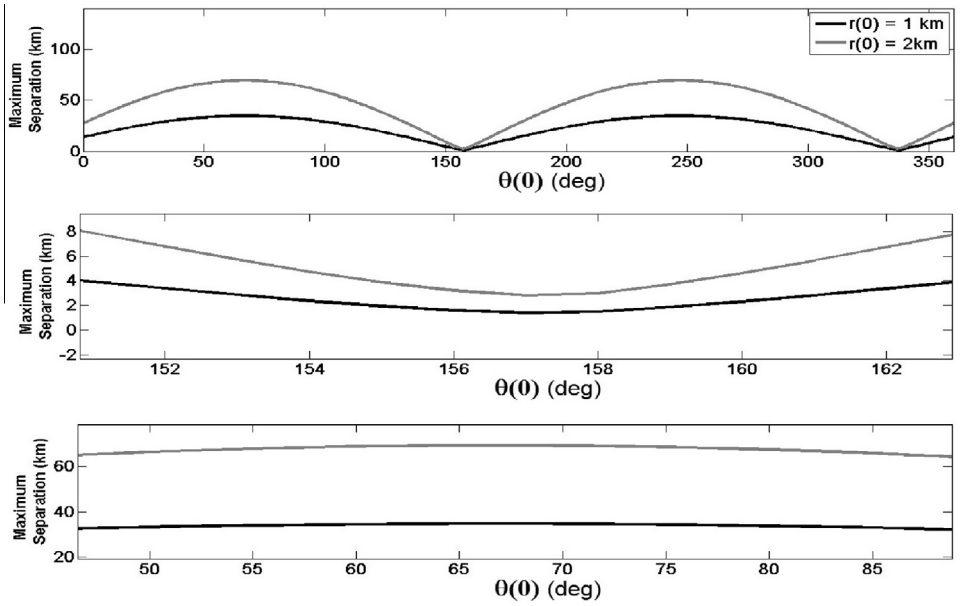

Fig. 29. Maximum separation (in km) during two years for $0^\circ \leqslant \theta(0) \leq 360^\circ$ and $r(0) = 1,\ 2$ km along the short period orbit shown in Fig. 7.

orbit around L_4, distributed in a similar fashion to the previous cases. The results are shown in Fig. 30. In the first row we see that the distance is a periodic function (period equal to 460 days for the long period orbit and 545 for the short period orbit) and that the maximum deviation from the starting separations is less than 2 km. Now, in the second row, the distances are periodic (period equal to 460 days for the long period orbit and 545 for the short period orbit) and the deviations from the periodic orbit are also increased by a factor of 40. Additionally, there is no difference between the qualitative and quantitative behavior of the distance for the trajectories starting at the same distance from $X_h(0)$.

Finally, Figs. 27 and 30 show that there exists a linear behavior between the distances for the trajectories starting at 1 km and 2 km from $X_h(0)$, i.e, the deviation for the trajectories starting at 1 km is half for the trajectories starting at 2 km from $X_h(0)$. Remember that this linear behaviour was also noted for the cost to maintain a spacecraft along the direction of zero, minimum and maximum relative radial acceleration. Therefore, there is no difference in the qualitative behavior of the distance for the trajectories starting at 1 km and 2 km from $X_h(0)$, and the spacecraft that start at those points probably remain aligned during the time span. To verify this fact, we compute the difference between the angles θ_1 and θ_2 at each instant t for all

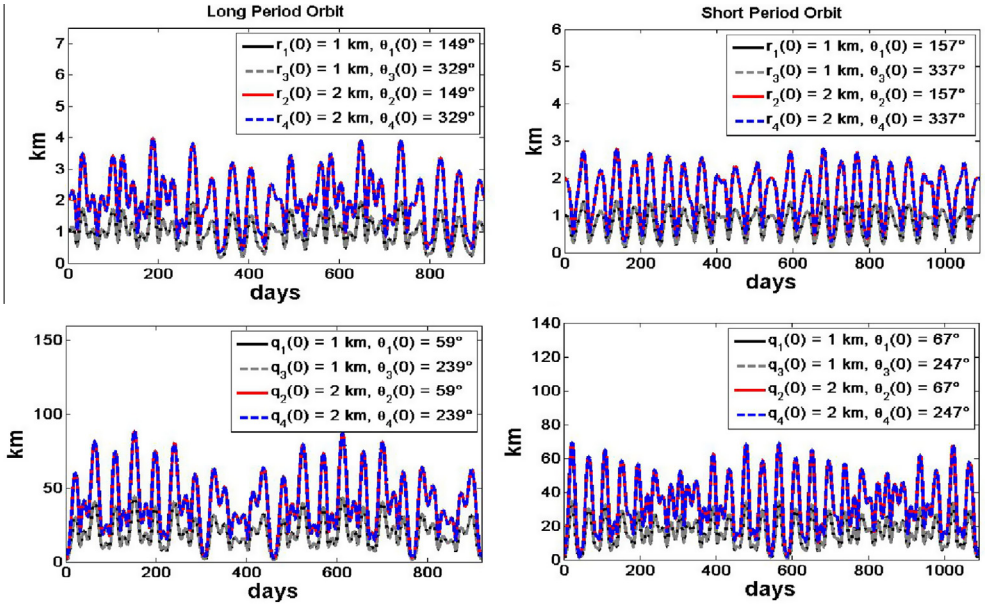

Fig. 30. Distance $d(X_h(t), X_i(t))$, between the trajectories of $\mathbf{r}_1$, $\mathbf{r}_2$, $\mathbf{r}_3$, $\mathbf{r}_4$ (first row), and $\mathbf{q}_1$, $\mathbf{q}_2$, $\mathbf{q}_3$, $\mathbf{q}_4$ (second row), and the long and short period orbits shown in Fig. 7.

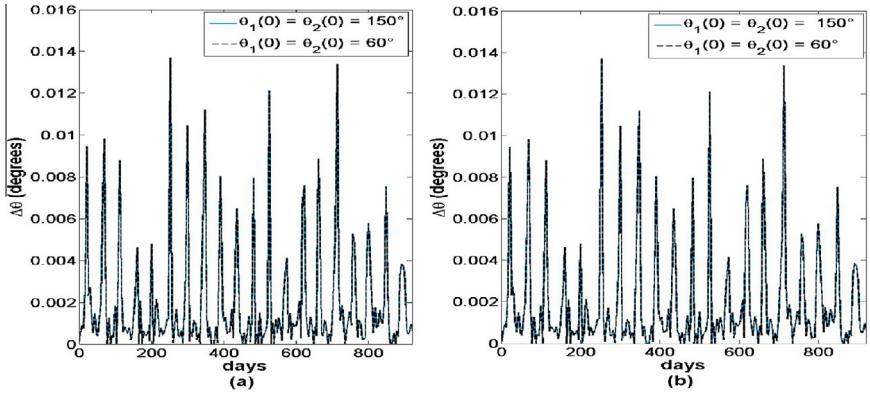

Fig. 31. Difference between the angles θ_1 and θ_2 at each instant t starting at 1 km and 2 km from $X_h(0)$ associated to the initial conditions of the long (a) and short (b) period orbits shown in Fig. 2.

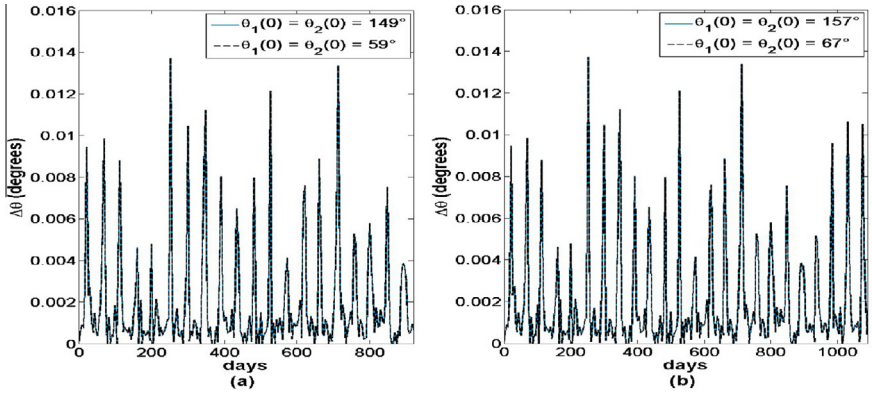

Fig. 32. Difference between the angles θ_1 and θ_2 at each instant t starting at 1 km and 2 km from $X_h(0)$ associated to the initial conditions of the long (a) and short (b) period orbits shown in Fig. 7.

previous trajectories starting at 1 km and 2 km from $X_h(0)$. In Fig. 31(a) and (b) we can see the results associated to the long and short period orbits shown in Fig. 2, respectively. Similarly, Fig. 32(a) and (b) show the results associated to the long and short period orbits shown in Fig. 7, respectively. As we can note, the difference of the angles θ_1 and θ_2 at each instant t is practically zero. Consequently, the spacecraft remain aligned along the periodic orbits around L_4, but their distances from the solution $X_h(t)$ oscillate periodically.

8. Conclusions

In this work we have shown that, considering the planar formation flight dynamics in the scenario of CRTBP, Zero Relative Radial Acceleration Lines (ZRRAL) do not exist for periodic orbits around equilateral equilibrium points when the amplitude of the periodic orbits is small enough. For these orbits, the relative position of the satellite has values for the angle θ such that its relative acceleration has either maximum or minimum radial component. On the other hand, the ZRRAL exist when the amplitude of the periodic orbits is large enough. However, for these orbits, the ZRRAL do not exist for every point of the periodic orbit. Therefore, in these cases, the relative position of the satellite has values for the angle θ such that its relative acceleration has maximum, minimum or zero radial component.

The cost estimate to maintain a satellite following an artificial trajectory has been determined by the integral of the residual acceleration. In the case of periodic orbits around L_4, it has been shown that the cost estimate is less when the relative position of the satellite points towards the direction where the radial component of the relative acceleration is minimum, although the ZRRAL do exist. Due to the fact that these regions appear and disappear along the periodic orbit, producing a discontinuity in the components of the relative velocity and acceleration and, therefore, a higher cost. On the other hand, the cost does not depend on the amplitude of the periodic orbit when the spacecraft follows the direction where the relative radial acceleration component is maximum. However, the cost increases with the amplitude when the spacecraft follows the direction where the radial acceleration component is minimum or zero. Similarly, we have computed the cost estimate to maintain a satellite when the relative position was fixed, i.e. when the angle θ remains constant along a family of periodic orbits around L_4. The function cost has a maximum at $\theta \approx 60^\circ$ and a minimum at $\theta \approx 150^\circ$.

A formation of three satellites has been studied. The configuration is a triangular geometry, such that the relative position along the periodic orbit is fixed and forms an equilateral triangle. The cost estimate to maintain this configuration is minimum when one of the satellites remains on the periodic orbit.

Note that in the force model defined by the CRTBP, the cost estimate to maintain the satellites in these configurations (ZRRAL, maximum or minimum radial acceleration, fixed angle) is very low. This fact is due to the stability of the periodic orbits around L_4, so that, particles that begin very close to a periodic orbit, their mutual distances will keep practically fixed, so the control applied to the spacecraft is very small. However, perturbations like solar radiation pressure, solar gravitational attraction and Moon's eccentricity affect the stability of the periodic orbits around L_4. Therefore, in subsequent works, all this kind of perturbations will be considered to compute a more accurate cost.

The dynamical behavior of the distance between a constellation of satellites and the periodic orbits around L_4 has also been determined. It can be seen that the maximum separation function does not depend on the initial condition taken along the periodic orbits and that this function has a period of 180°. Similarly, the best position to reduce the maximum separation is about $\theta = 150^\circ$. On the other hand, the position that increase the maximum separation is about $\theta = 60^\circ$. Thus, placing satellites in the directions of either minimum or maximum deviation from the starting separations, the distance from the periodic orbit behaves as a periodic function in such a way that the satellites remain aligned. Therefore, if we want to maintain fixed the configuration, a thrust would be necessary only to control the separation. In the case of minimum deviation, since the deviation in some cases was less than 2 km, the cost estimate to maintain the distance fixed would be very small. Therefore, simulations have shown that the direction of minimum radial component defines the initial conditions for the satellites with respect to the periodic orbit around L_4 so that the drift between them be minimized. This information has a practical value for the control of the formation flying since the fuel spent will be less if the spacecraft are set up in the direction where the relative radial acceleration component is minimum.

Acknowledgments

Firstly, the authors would like to thank the use of EIXAM, the UPC Applied Math cluster system for research computing (see <http://www.ma1.upc.edu/eixam/>), provided during the international research stage in Barcelona from which this work was the result. The authors are also grateful to the Fapesp (Fundação de Amparo à Pesquisa do Estado de São Paulo), processes 2008/06066-5, 2011/08171-3, 2011/50151-0, and 2013/03233-6, and the CNPq (Conselho Nacional para Desenvolvimento Científico e Tecnológico, Brazil), for financial support. Finally, prof. J. J. Masdemont thanks the MINECO-FEDER grant MTM 2012-31714 and the Catalan grant 2009SGR-D-D589-E.

References

Alfriend, K.T., Gim, D-W., Vadali, S.R., 2002. The characterization of formation flight satellite relative motion orbits. AAS/AIAA Spaceflight Mech. Mtg. San Antonio, Texas. Paper AAS 02-143.

Barry, S., 2007. Analytical Conics. Dover Publ., New York.
Battrick, B., 2000. XEUS Steering Committee: X-Ray Evolving-Universe Spectroscopy: The XEUS Mission Summary. ESA Publications Division, Noordwijk, The Netherlands.
Breakwell, J.V., Brown, J., 1979. The Halo family of 3-dimensional periodic orbits in the Earth–Moon restricted 3-body problem. Celest. Mech. 20 (4), 389–404. http://dx.doi.org/10.1007/BF01230405.
Bristow, J., Folta, D., Hartman, K., 2000. A formation flying technology vision. AIAA Space Conf., Long Beach, CA. AIAA Paper No. 2000-5194.
Burns, R., McLaughlin, C.A., Leitner, J., et al., 2000. TechSat 21: formation design, control, and simulation. IEEE Aero. Conf.
Carter, T., Humi, M., 2002. Clohessy–Wiltshire equations modified to include quadratic drag. J. Guid. Control Dyn. 25 (6), 1058–1063. http://dx.doi.org/10.2514/2.5010.
Cash, W., Kendrick, S., Noecker, C., et al., 2009. The new worlds observer: the astrophysics strategic mission concept study. Proc. SPIE vol. 7436, 14. http://dx.doi.org/10.1117/12.827486, article id. 743606.
Catlin, K.A., McLaughlin, C.A., 2007. Earth–Moon triangular libration point spacecraft formations. J. Spacecraft Rockets 44 (3), 660–670. http://dx.doi.org/10.2514/1.20152.
Clohessy, W., Wiltshire, R., 1960. Terminal guidance system for satellite rendezvous. J. Aerosp. Sci. 27 (9), 653–678. http://dx.doi.org/10.2514/8.8704.
Danby, J.M.A., 1962. Fundamentals of Celestial Mechanics. Willmann-Bell Inc., Virginia, USA.
Defilippi, G., Jr. 1977. Station Keeping at the L4 Libration Point: A Three Dimensional Study (M.Sc. thesis). School of Engineering, Air Force Inst. of Tech., Wright-Patterson AFB, OH.
Faquhar, R.W., 1968. The Control and Use of Libration-Point Satellites (Ph.D. thesis). Dept. of Aeronautics and Astronautics, Stanford University.
Flick, M., 01 Nov. 2012. Earth Observing-1: Preliminary Technology and Science Validation Report. Goddard Space Flight Center. <http://eo1.gsfc.nasa.gov/new/validationReport/index.html>.
Fridlund, C.V.M., Capaccioni, Fabrizio, 2002. Infrared space interferometry-the DARWIN mission. Adv. Space Res. 30 (9), 2135–2145. http://dx.doi.org/10.1016/S0273-1177(02)00585-9.
Gill, E., Montenbruck, O., D'Amico, S., 2007. Autonomous formation flying for the PRISMA mission. J. Spacecraft Rockets 44 (3), 671–681. http://dx.doi.org/10.2514/1.23015.
Gómez, G., Llibre, J., Martínez, R., et al., 1987. Study on Orbits near the Triangular Libration Points in the perturbed Restricted Three-Body Problem, ESOC Contract 6139/84/D/JS(SC), Final Report, IV +238 p.
Gómez, G., Jorba, À., Masdemont, J., et al., 1993. Study of the transfer from the Earth to a Halo orbit around the equilibrium point L1. Celest. Mech. Dyn. Astron. 56 (4), 541–562. http://dx.doi.org/10.1007/BF00696185.
Gómez, G., Llibre, J., Martínez, R., et al., 2000. Dynamics and mission design near libration points. Fundamentals: The Case of Collinear Libration Points, vol. I. World Scientific Publishing Co., Inc., Singapore.
Gómez, G., Jorba, À., Masdemont, J., et al., 2001. Dynamics and mission design near libration points, . Advanced Methods for Triangular Points, first ed., vol. IV. World Scientific Publishing Co., Inc., Singapore.
Gómez, G., Marcote, M., Masdemont, J.J., et al., 2006. Natural configurations and controlled motions suitable for formation flying (AAS 05–347). Adv. Astronaut. Sci. 123 (2), 1513–1530.
Hellman, H., Persson, S., Larsson, B., Oct. 2009. PRISMA, a Formation Flying Mission on the Launch Pad. 60th Int. Astro. Congress, Daejeon, Republic of Korea.
Henon, M., 1973. Vertical stability of periodic orbits in the restricted problem. Astron. Astrophys. 28, 415–426.
Hill, G., 1878. Researches in the lunar theory. Am. J. Math. 1, 5–26.
Howell, K.C., 1984. Three-dimensional, periodic, Halo orbits. Celest. Mech. 32 (1), 53–71. http://dx.doi.org/10.1007/BF01358403.
Hsiao, F.Y., Scheeres, D.J., 2002. The dynamics of formation flight about a stable trajectory. J. Astronaut. Sci. 50 (3), 269–287.
Humi, M., Carter, T., 2006. Closed-form solutions for near-circular arcs with quadratic drag. J. Guid. Control Dyn. 29 (3), 513–518. http://dx.doi.org/10.2514/1.16186.
Kamel, A.A., Breakwell, J.V., 1970. Stability of motion near Sun-perturbed Earth–Moon triangular points. In: Giacaglia, G.E.O. (Ed.), Periodic Orbits, Stability and Resonances. Reidel, pp. 82–90.
Kapila, V., Sparks, A.G., Buffington, J.M., et al., 2000. Spacecraft formation flying: dynamics and control. J. Guid. Control Dyn. 23 (3), 561–564. http://dx.doi.org/10.2514/2.4567.
Lawrence, J.D., 1972. A Catalog of Special Plane Curves. Dover Publ., New York.
McLaughlin, C.A., Catlin, K., Sept. 2004. Perturbation Analysis for Spacecraft Formations Near the Earth–Moon Triangular Libration Points. Proc. 2nd International Symposium on Formation Flying Missions and Technologies CD-ROM, Washington, D.C., NASA CP-2005-212781.
Miele, A., 1960. Theorem of image trajectories in the Earth–Moon space. Astron. Acta 6, 225–232.
O'Neill, G.K., 1974. The colonization of space. Phys. Today 27 (9), 32–40. http://dx.doi.org/10.1063/1.3128863.
Persson, S., Bodin P., Gill, E., et al., 2006. PRISMA An Autonomous Formation Flying Mission. Proc. Small Satellite Systems and Services Symp. Sardinia, Italy, pp. 25–29.
Persson, S., D'Amico, S., Harr, J., Sept. 2010. Flight Results from PRISMA Formation Flying and Rendezvous Demonstration. 61st Int. Astro. Congress, Prague, Czech Republic.
Peterseim, M., Robertson, D.I., Danzmann, K., et al., 2000. LISA interferometer sensitivity to spacecraft motion. Adv. Space Res. 25 (6), 1143–1147. http://dx.doi.org/10.1016/S0273-1177(99)00975-8.
Sabol, C., Burns, R., McLaughlin, C.A., 2001. Satellite formation flying design and evolution. J. Spacecraft Rockets 38 (2), 270–278. http://dx.doi.org/10.2514/2.3681.
Schechter, H.B., 1968. Three-dimensional nonlinear stability analysis of Sun-perturbed Earth–Moon equilateral points. AIAA J. 6 (7), 1223–1228. http://dx.doi.org/10.2514/3.4725.
Schutz, B.E., 1977. Orbital Mechanics of Space Colonies at L4 and L5 of the Earth–Moon System. AIAA Astro. Specialist Conf., Los Angeles, CA., Jan. AIAA Paper No. 77–33.
Sengupta, P., Vadali, S.R., 2007. Relative motion and the geometry of formations in Keplerian elliptic orbits. J. Guid. Control Dyn. 30 (4), 953–964. http://dx.doi.org/10.2514/1.25941.
Sengupta, P., Vadali, S.R., Alfriend, K.T., 2007. Second-order state transition for relative motion near perturbed, elliptic orbits. Celest. Mech. Dyn. Astr. 97 (2), 101–129. http://dx.doi.org/10.1007/s10569-006-9054-5.
Sholomitsky, G.B., Prilutsky, O.F., Rodin, V.G., 1977. Infra-red space interferometer. 28th Int. Astro. Fed. Congress, Praha, Czechoslovakia. Paper IAF-77-68.
Szebehely, V., 1967. Theory of Orbits. Academic Press, New York, NY.
Tapley, B.D., Schultz, B.E., 1970. Numerical studies of solar influenced particle motion near triangular Earth–Moon libration points. In: Giacaglia, G.E.O. (Ed.), Periodic Orbits, Stability and Resonances. Reidel, pp. 128–142.
Ticker, R.L., Azzolini, J.D., 2000. Survey of Distributed Spacecraft Technologies and Architectures for NASA's Earth Science Enterprise in the 2010–2015 Timeframe. NASA/TM-2000-209964, Aug. 2000.
Wong, F.Y.W., 2009. Formation-Keeping Strategies At The Earth–Moon L4 Triangular Libration Point (M.A.Sc. thesis). Department of Aerospace Engineering, Ryerson University, Toronto, Ontario, Canada.